GSA Data Repository 2016205

Empirical constraints of shock features in monazite using shocked zircon inclusions

Erickson et al.

DR 1 Analytical methods

Identification of Shocked Monazites and Imaging External Shock Features

Heavy minerals were separated from loose sediment samples collected within the Vaal River basin and grains were identified after the methods of Cavosie et al. (2010) and Erickson et al. (2013). Organics were washed from the samples and then the samples were processed with the heavy liquid Acetylene tetra-bromide to separate the heavy mineral fraction. The heavy mineral fractions were further divided using a Frantz isodynamic magnetic separator. Following which monazites were mounted on Carbon tape on 1 cm Aluminum scanning electron microscope (SEM) stubs. Exterior surface images of the detrital monazites were collected using a Cambridge Instruments Stereoscan 120 SEM at the University of Puerto Rico Mayagüez (UPRM), a Hitachi S-3400 at the University of Wisconsin, Madison (UW), and a JEOL 5610LV SEM at Oberlin College. Energy dispersive spectra (EDS) were collected from the monazites to confirm their composition using the SEMs at UW and Oberlin.

Imaging Internal Shock Features

After exterior microstructures of shocked monazite and zircon were imaged, they were cast and polished in 2.54-cm epoxy grain mounts. The grain mounts were first given a 1 μm diamond polish before being given a chemical-mechanical polish with a colloidal dispersion of 5 nm silica in NaOH. After polishing, internal textures of the deformed monazites were imaged using the Tescan Mira3 field emission (FE) SEM at the Microscopy & Microanalysis Facility, within the John de Laeter Centre for Isotope Research (JDL), Curtin University, Western

Australia. Backscattered electron photomicrographs of the monazites were collected using an accelerating voltage of 15 kV. Zircon inclusions were identified using EDS with an accelerating voltage of 20 kV and were imaged by panchromatic cathodoluminescence (CL) with an accelerating voltage of 10 kV. BSE and CL photomicrographs from all shock monazite and zircon inclusions are included in Data Repository item 2.

EBSD Mapping of Monazites and Zircons

Deformed monazites and zircons were subsequently mapped by EBSD. Electron backscatter patterns (EBSPs) were collected from the monazites and zircons in orthogonal grids using a Nordsly Nano high resolution detector and Oxford Instruments Aztec 2.4 acquisition software package on the Mira3 FEG-SEM. EBSD analyses were collected with a 20 kV accelerating voltage, 70° sample tilt, ~20 mm working distance, and 18 nA beam current. Post-processing the EBSD data was undertaken with Oxford Instruments Channel 5.11 software suite. Zircons were mapped using the match unit Zircon 5260 after the methods of Reddy et al. (2007) while monazites were mapped with the match unit described in Erickson et al. (2015), which originates from crystallographic data of Ni et al. (1995). Operating conditions and noise reduction parameters are summarized in Data Repository Table 1. EBSD maps were produced using the Tango suite of Channel5, while pole figures were processed in Mambo suite of Channel5. EBSD maps and pole figures of the shocked monazite and zircon pairs can be found in Data repository 2. Shock textures of the monazites and zircons are summarized in Data Repository Table 2, in which the following maps, produced with Tango, can be found:

1. crystallographic orientation map using all Euler color scheme
2. special boundary maps in which boundaries between adjacent pixels are color coded if they matched a specific misorientation axis and angle pair, within 5°, consistent

with a twin boundary. Inverse Pole Figure (IPF) color scheme was added to each zircon in this figure.

3. Texture component map of the shocked monazite, which show up to 20° of misorientation from the mean orientation of the host grain. The mean orientation, as Euler angles, was measured using the "grain detect" component of Tango. Zircons are colored in fuchsia to highlight their locations within the host monazite.
4. Local misorientation map displaying amount of misorientation between each pixel and the surrounding 3 X 3 grid.

Conversion of EBSD disorientation data to deformation twins

Crystallographic orientation data obtained by EBSD can be used to calculate the misorientation between two different crystallographic orientations. This is commonly expressed as three superimposed rotations about axes specified by a convention, where the rotation angles are known as Euler angles, or a single angular rotation around a stated axis (angle-axis pair). Depending on the crystal symmetry there may be more than one angle-axis pair that achieves the same rotation but the rotation angles will be different. The disorientation convention used in this paper means that the angle-axis pair with the smallest angular rotation is chosen from all the symmetrically equivalent rotations. For monoclinic minerals, of which monazite is one, there are only two symmetric equivalents. This arises from the diad axis of symmetry parallel to the [010] direction and the fact that EBSD data can only describe proper rotations (i.e. the mirror plane perpendicular to [010] is not a proper rotation).

While the disorientation can be used to document twin microstructures, it is often cryptic and not geometrically meaningful. The relationship between two parts of a twin can be described by one (or both) of two 180° rotations that are geometrically related to either the composition

plane, K1 or shear direction, η1 (summarized in Figure A1 after Christian and Mahajan, 1995). For type 1 twins, the twin is related to the host by a 180° rotation around the pole to (a rational) K1. For type 2 twins, the twin is related to the host by a 180° rotation around (a rational) η1. Composite twins satisfy both constraints.

To document the nature of the twins observed in monazite and identify the composition planes pairs of Euler angles from twin and host were used to calculate not only the disorientation axis but also its symmetrical equivalent. In each case, except one, the misorientation calculation revealed a 180° rotation that was not always apparent from the disorientation. Where the 180° rotation axis was close to a pole to a rational plane this was noted to be a type 1 twin relationship and where it was close to a rational crystallographic direction the twin was documented as a type 2 relationship. For a number of twins (those with a disorientation rotation of 180°) both of these criteria were satisfied and they were noted to be composite twins. The procedure was implemented in Matlab as follows using the unit cell parameters of natural monazite after Ni et al. (1995):

1. Constructs a list of directions and planes in the crystal reference frame, removing collinear ones (e.g. 111 and 222).
2. Calculates the x,y,z orientation of each of the directions and plane normal for a crystal with Euler angles (0 0 0). This takes into account the crystal unit cell parameters.
3. Calculate the symmetry operators (Si) for the Laue group. In this case there are only 2 symmetrical equivalents which are related by a 180 rotation around [0 1 0].
4. For each pair of sets of Euler angles do the following:
    a. Calculate the rotation matrix (DCM) for each Euler angle triple using equations B2 and B4 of Cho et al. (2005)

b. Calculate the rotation from one to the other (DCM3 = DCM2 – DCM1)

c. Calculate the rotation matrix for each symmetric equivalent (DCM3i = Si x DCM3)

d. Calculate the angle and axis (in Cartesian x,y,z co-ordinates) of rotation for each resulting rotation matrix

e. Calculate the crystallographic index of each rotation axis. This approach gives the closest zone axis. It should be noted that where the rotation axis is a pole to a plane then it is not necessarily a rational direction (especially in monoclinic minerals where only (010)=[010]).

f. For a list of planes from where {h, k, l} are integers from -3 to 3 calculate the angle in x,y,z co-ordinates between the rotation axis and the plane normal (using dot product of unit vectors). If the angle is >90 then use the supplementary angle thereby ignore polarity of the poles to planes i.e. (001) = (00-1).

g. Compile the data into an output format giving the angle and axis (in x,y,z) for each symmetric variant, crystallographic vector (with smallest value normalised to 1), angle between rotation axis and closest direction, closest direction, angle between rotation axis and closest pole to plane, closest pole plane.

The input parameters and results of the script are summarized in DR3.

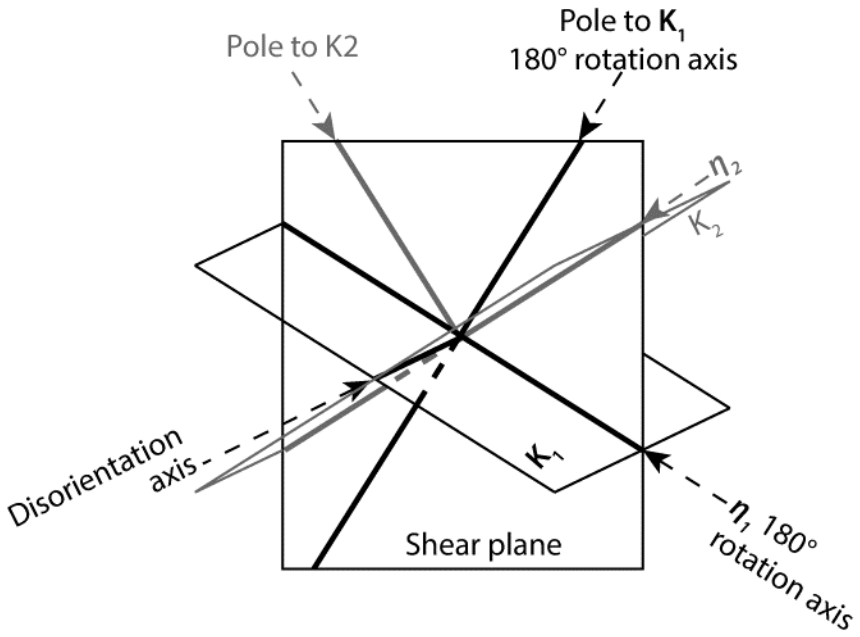

Figure A1. Twin mode conventions modified after Christian and Mahjan (1995)

Data Repository Table 1.1 EBSD analytical conditions grain 07VD07-39

Figure	07VD07-39 wholegrain	07VD07-39 Z1	07VD07-39 Z1 AOI 1	07VD07-39 Z2	07VD07-39 Z2 AOI 1
Acquisition speed (Hz)	40	40	40	40	40
Background (frames)	64	64	64	64	64
Binning	4x4	4x4	4x4	4x4	4x4
Gain	High	High	High	High	High
Hough resolution	60	60	60	60	60
Band detection min/max	6/8	6/8	6/8	6/8	6/8
Mean angular deviation (monazite)	0.4439	0.4397		0.4595	
Mean angular deviation (zircon)	0.2772	0.3041	0.2919	0.281	0.3045
X steps	540	176	41	159	28
Y steps	406	168	131	174	52
Step distance (μm)	1	0.25	0.05	0.2	0.05
Noise reduction – 'wildspike'	Yes	No	No	No	No
n neighbour zero solution extrapolation	7	7	7	7	7
Kuwahara Filter	-	-	-	-	-
SEM MODEL: Tescan Mira3 FEG-SEM					
EBSD camera: Nordsly nano high resolution detector					
Acquisition software: Aztec 2.4					
Carbon coat (<5nm)	Yes	Yes	Yes	Yes	Yes
Acc. Voltage (kV)	20	20	20	20	20
Working distance (mm)	20	20	20	20	20
Tilt (degrees)	70	70	70	70	70

Data Repository Table 1.2 EBSD analytical conditions grain 07VD07-39 continued

Figure	07VD07-39 z3	07VD07-39 Z4	07VD07-39 Z5	07VD07-39 Z6	07VD07-39 Z7, 8
Acquisition speed (Hz)	40	40	40	40	40
Background (frames)	64	64	64	64	64
Binning	4x4	4x4	4x4	4x4	4x4
Gain	High	High	High	High	High
Hough resolution	60	60	60	60	60
Band detection min/max	6/8	6/8	6/8	6/8	6/8
Mean angular deviation (monazite)	0.4537	0.4061	0.3841	0.3457	0.4822
Mean angular deviation (zircon)	0.2672	0.2766	0.2658	0.2752	0.3126
X steps	185	48	80	70	108
Y steps	116	124	58	60	78
Step distance (μm)	0.5	0.5	0.3	0.25	0.5
Noise reduction – 'wildspike'	Yes	Yes	Yes	Yes	Yes
n neighbour 0 solution extrapolation	7	7	7	7	7
Kuwahara Filter	-	-	-	-	-
SEM MODEL: Tescan Mira3 FEG-SEM					
EBSD camera: Nordsly nano high resolution detector					
Acquisition software: Aztec 2.4					
Carbon coat (<5nm)	Yes	Yes	Yes	Yes	Yes
Acc. Voltage (kV)	20	20	20	20	20
Working distance (mm)	20	20	20	20	20
Tilt (degrees)	70	70	70	70	70

Data Repository Table 1.3 EBSD analytical conditions grain 07VD07-67

Figure	07VD07-67 wholegrain	07VD07-67 Z1	07VD07-67 Z1 AOI
Acquisition speed (Hz)	40	40	40
Background (frames)	64	64	64
Binning	4x4	4x4	4x4
Gain	High	High	High
Hough resolution	60	60	60
Band detection min/max	6/8	6/8	6/8
Mean angular deviation (monazite)	0.4166	0.6064	0.5768
Mean angular deviation (zircon)	0.4418	0.5878	0.6009
X steps	386	178	98
Y steps	439	139	203
Step distance (μm)	1.5	0.15	0.05
Noise reduction – 'wildspike'	Yes	Yes	No
n neighbor 0 solution extrapolation	7	7	7
Kuwahara Filter	-	-	-
SEM MODEL: Tescan Mira3 FEG-SEM EBSD camera: Nordsly nano high resolution detector Acquisition software: Aztec 2.4			
Carbon coat (<5nm)	Yes	Yes	Yes
Acc. Voltage (kV)	20	20	20
Working distance (mm)	20	20	20
Tilt (degrees)	70	70	70

Data Repository Table 1.4 EBSD analytical conditions grain 09VD58-166

Figure	09VD58-166 wholegrain	09VD58-166 zircons	09VD58-166 Z1 AOI	09VD58-166 Z2
Acquisition speed (Hz)	40	40	40	40
Background (frames)	64	64	64	64
Binning	4x4	4x4	4x4	4x4
Gain	High	High	High	High
Hough resolution	60	60	60	60
Band detection min/max	6/8	6/8	6/8	6/8
Mean angular deviation (monazite)	0.4701	0.4855	0.6493	0.5445
Mean angular deviation (zircon)	0.4995	0.4706	0.3999	0.576
X steps	435	135	84	79
Y steps	330	109	67	78
Step distance (μm)	0.45	0.4	0.1	0.1
Noise reduction – 'wildspike'	Yes	Yes	Yes	No
n neighbor zero solution extrapolation	7	7	7	7
Kuwahara Filter	-	-	-	-
SEM MODEL: Tescan Mira3 FEG-SEM				
EBSD camera: Nordsly nano high resolution detector				
Acquisition software: Aztec 2.4				
Carbon coat (<5nm)	Yes	Yes	Yes	Yes
Acc. Voltage (kV)	20	20	20	20
Working distance (mm)	20	20	20	20
Tilt (degrees)	70	70	70	70

Data Repository Table 1.5 EBSD analytical conditions grain 07VD07-4

Figure	07VD08-4 wholegrain	07VD08-4 Z1	07VD08-4 Z1 AOI	07VD08-4 Z2
Acquisition speed (Hz)	40	40	40	40
Background (frames)	64	64	64	64
Binning	4x4	4x4	4x4	4x4
Gain	High	High	High	High
Hough resolution	60	60	60	60
Band detection min/max	6/8	6/8	6/8	6/8
Mean angular deviation (monazite)	0.6028	0.3898	0.796	0.4551
Mean angular deviation (zircon)	0.4926	0.2989	0.2856	0.4322
X steps	748	154	122	81
Y steps	760	141	113	84
Step distance (μm)	0.6	0.5	0.1	0.25
Noise reduction – 'wildspike'	Yes	Yes	No	Yes
n neighbor zero solution extrapolation	7	7	7	7
Kuwahara Filter	-	-	-	-
SEM MODEL: Tescan Mira3 FEG-SEM				
EBSD camera: Nordsly nano high resolution detector				
Acquisition software: Aztec 2.4				
Carbon coat (<5nm)	Yes	Yes	Yes	Yes
Acc. Voltage (kV)	20	20	20	20
Working distance (mm)	20	20	20	20
Tilt (degrees)	70	70	70	70

Data Repository Table 1.6 EBSD analytical conditions grains 09VD16-50, 09VD16-65

Figure	09VD16-50	09VD16-65	09VD16-65 z1	09VD16-65 z1 AOI
Acquisition speed (Hz)	40	40	40	40
Background (frames)	64	64	64	64
Binning	4x4	4x4	4x4	4x4
Gain	High	High	High	High
Hough resolution	60	60	60	60
Band detection min/max	6/8	6/8	6/8	6/8
Mean angular deviation (monazite)	0.7031	0.4036	0.6635	
Mean angular deviation (zircon)	0.5387	0.3609	0.5752	0.5745
X steps	1181	547	225	50
Y steps	1072	489	209	72
Step distance (μm)	0.3	0.4	0.2	0.1
Noise reduction – 'wildspike'	Yes	Yes	Yes	No
n neighbor zero solution extrapolation	7	7	7	7
Kuwahara Filter	-	-	-	-
SEM MODEL: Tescan Mira3 FEG-SEM				
EBSD camera: Nordsly nano high resolution detector				
Acquisition software: Aztec 2.4				
Carbon coat (<5nm)	Yes	Yes	Yes	Yes
Acc. Voltage (kV)	20	20	20	20
Working distance (mm)	20	20	20	20
Tilt (degrees)	70	70	70	70

Data Repository Table 1.7 EBSD analytical conditions grains 09VD16-68 and 09VD53-26

Figure	09VD16-68	09VD16-68 AOI	09VD16-68 Z1	09VD16-68 Z2	09VD53-26
Acquisition speed (Hz)	40	40	40	40	40
Background (frames)	64	64	64	64	64
Binning	4x4	4x4	4x4	4x4	4x4
Gain	High	High	High	High	High
Hough resolution	60	60	60	60	60
Band detection min/max	6/8	6/8	6/8	6/8	6/8
Mean angular deviation (monazite)	0.4413	0.6846	0.7411	0.6392	0.5608
Mean angular deviation (zircon)	0.3609	0.5403	0.5368	0.5662	0.4849
X steps	520	175	192	170	1767
Y steps	503	216	293	212	1089
Step distance (μm)	0.4	0.2	0.07	0.1	0.2
Noise reduction – 'wildspike'	Yes	Yes	Yes	Yes	Yes
n neighbor zero solution extrapolation	7	7	7	7	7
Kuwahara Filter	-	-	-	-	-
SEM MODEL: Tescan Mira3 FEG-SEM					
EBSD camera: Nordsly nano high resolution detector					
Acquisition software: Aztec 2.4					
Carbon coat (<5nm)	Yes	Yes	Yes	Yes	Yes
Acc. Voltage (kV)	20	20	20	20	20
Working distance (mm)	20	20	20	20	20
Tilt (degrees)	70	70	70	70	70

Data Repository Table 2.1 Detrital shocked monazite microstructures

Grain	Length (μm)	Width (μm)	zrn incs.	shocked zircons	# of twin sets	95° / <201> (1)	95° / <201> (2)	180° / <001>	180° /<100>	180° / <101>	94° /<001>	180° / <201>	147° / <10-1>	107° / <41-1>	55° / <001>	85° / <401>	91° <104>	Planar Def. Bands	micro gran-ules
07VD07 M67	650	510	1	1	3	1		1	1									2	
07VD07 M39	550	385	8	2	6	1	1	1	1	1	1							1	
07VD08 m1 M4	445	365	2	1	8	1	1	1	1	1		1	1	1		1	1	2	
09VD16 m3 M50	375	295	1	1	6	1	1	1	1	1	1							2	
09VD53 m3 M26	360	195	1	1	5	1	1	1	1	1								2	yes
09VD16 m3 M65	200	155	1	1	3	1	1		1									1	
09VD16 m3 M68	200	150	2	1	7	1	1	1	1	1	1				1			2	yes
09VD58 m1 M166	-	-	2	1	4	1		1	1	1								1	yes
Total (*mean*)	*397*	*293*	18	9		8	6	7	8	6	3	1	1	1	1	1	1	13	3

Data Repository Table 2.2 Microstructures of detrital zircon inclusions

Grain	Zircon	Length (μm)	Width (μm)	CL pattern	shocked zircon	Sets of {112} Microtwins	{100} PDBs
07VD07 M39	1	45	26	Oscillatory	yes	3	
	2	32	28	Oscillatory	yes	3	
	3	91	48	Oscillatory			
	4	54	15	Oscillatory			
	5	24	10.5	Sector			
	6	16	12	Oscillatory			
	7	28.5	15	Oscillatory			
	8	23	19.5	Oscillatory			
07VD07 M67	1	26	16	Oscillatory	yes	2	
09VD58 m1 M166	1	40	12	Oscillatory			
	2	6.5	4.6	dark	yes	1	
07VD08 m1 M4	1	90	30	Oscillatory	yes	1	
	2	15	9	Oscillatory			
09VD16 m3 M50	1	39	34.5	Oscillatory	yes	1	
09VD16 m3 M65	1	39	14	Oscillatory	yes	1	
09VD16 m3 M68	1	17	10.5	dark	yes	1	
	2	19	9	Oscillatory			
09VD53 m3 M26	1	27	24	Oscillatory	yes		2
Total (*mean*)	18	*35*	*19*		9		

REFERENCES

Cavosie, A. J., Quintero, R. R., Radovan, H. A., and Moser, D. E., 2010, A record of ancient cataclysm in modern sand: Shock microstructures in detrital minerals from the Vaal River, Vredefort Dome, South Africa: Geological Society of America Bulletin, v. 122, no. 11-12, p. 1968-1980.

Cho, J.-H., Rollett, A. D., and Oh, K. H., 2005, Determination of a mean orientation in electron backscatter diffraction measurements: Metallurgical and Materials Transactions A, v. 36, no. 12, p. 3427-3438.

Christian, J. W., and Mahajan, S., 1995, Deformation twinning: Progress in Materials Science, v. 39, no. 1–2, p. 1-157.

Erickson, T. M., Cavosie, A. J., Moser, D. E., Barker, I. R., Radovan, H. A., and Wooden, J., 2013, Identification and provenance determination of distally transported, Vredefort-derived shocked minerals in the Vaal River, South Africa using SEM and SHRIMP-RG techniques: Geochimica et Cosmochimica Acta, v. 107, no. 0, p. 170-188.

Erickson, T. M., Pearce, M. A., Taylor, R. J. M., Timms, N. E., Clark, C., Reddy, S. M., and Buick, I. S., 2015, Deformed monazite yields high-temperature tectonic ages: Geology, v. 43, no. 5, p. 383-386.

Ni, Y., Hughes, J. M., and Mariano, A. N., 1995, Crystal chemistry of the monazite and xenotime structures: American Mineralogist, v. 80, no. 1, p. 21-26.

Reddy, S. M., Timms, N. E., Pantleon, W., and Trimby, P., 2007, Quantitative characterization of plastic deformation of zircon and geological implications: Contributions to Mineralogy and Petrology, v. 153, no. 6, p. 625-645.

07VD07 - Monazite 39

Rietspruit tributary

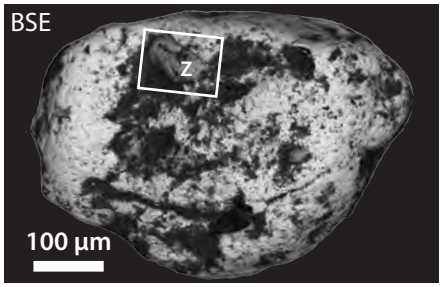

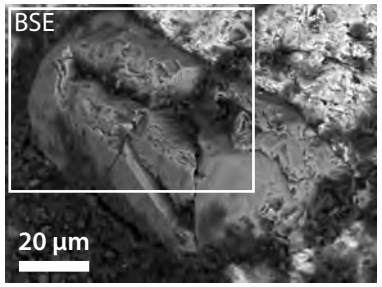

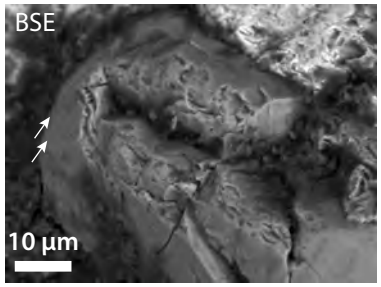

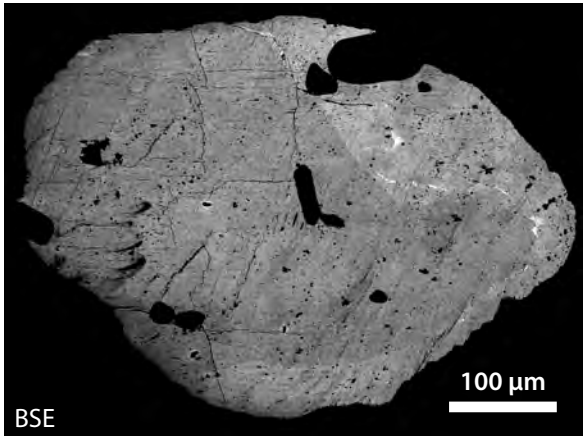

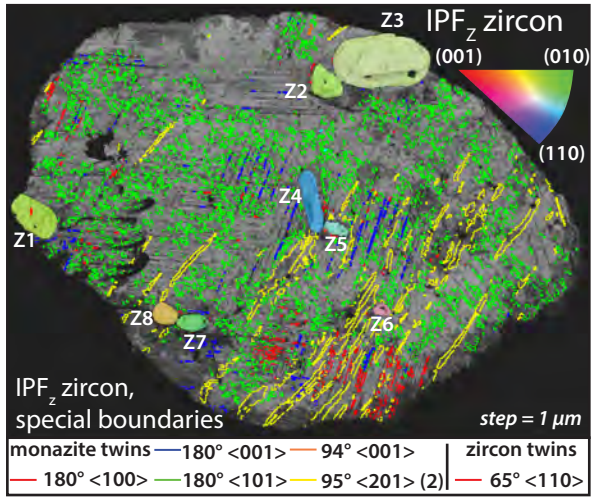

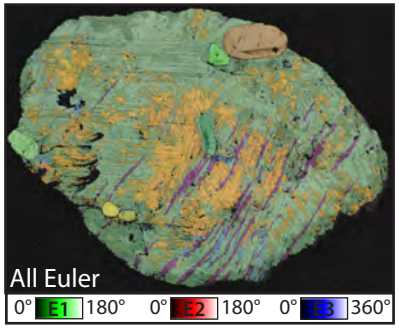

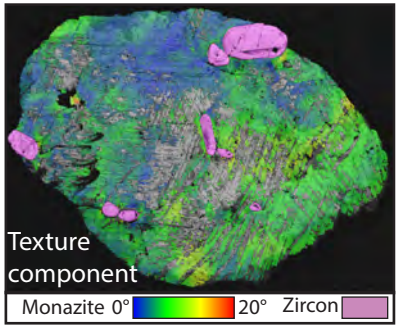

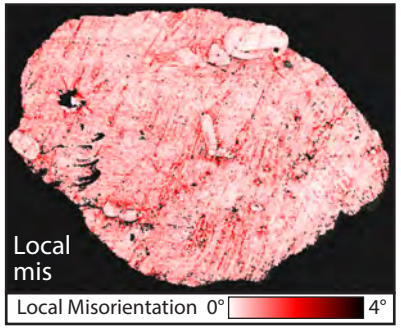

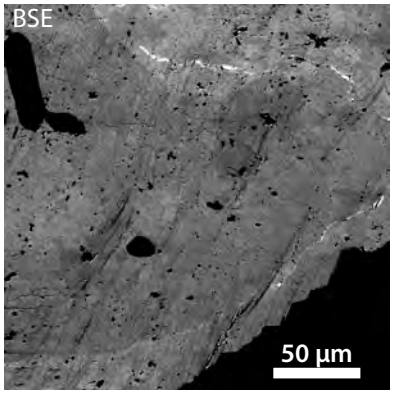

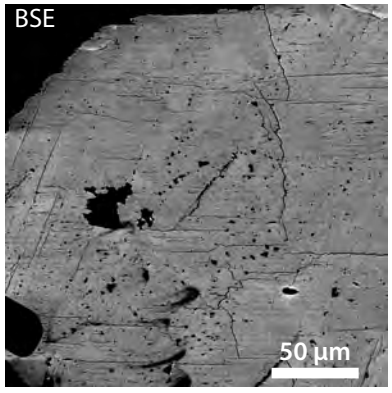

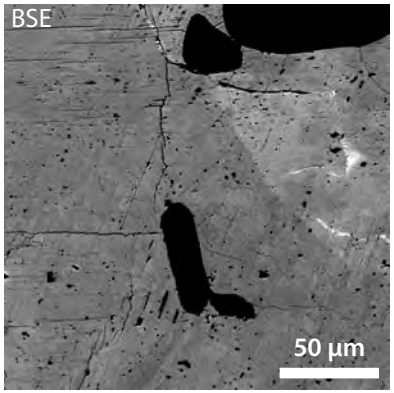

Pole figures - monazite
All Euler coloring

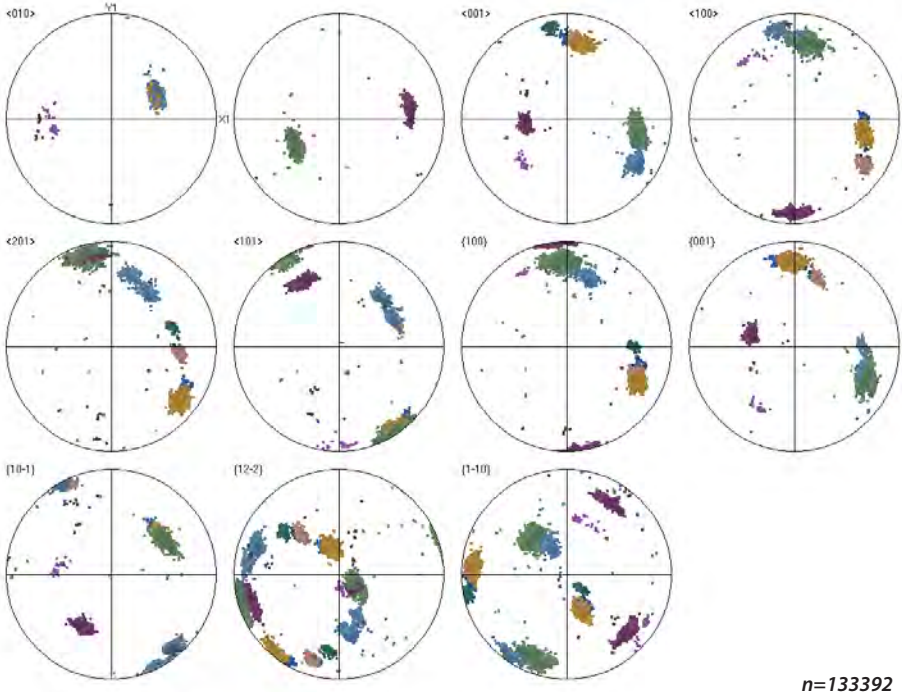

Pole figures - zircon inclusions (n=8)
IPFz Coloring

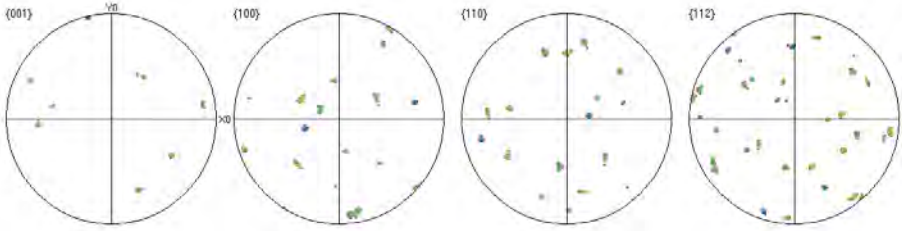

07VD07 - Monazite 39 cont.

Zircon Inclusions

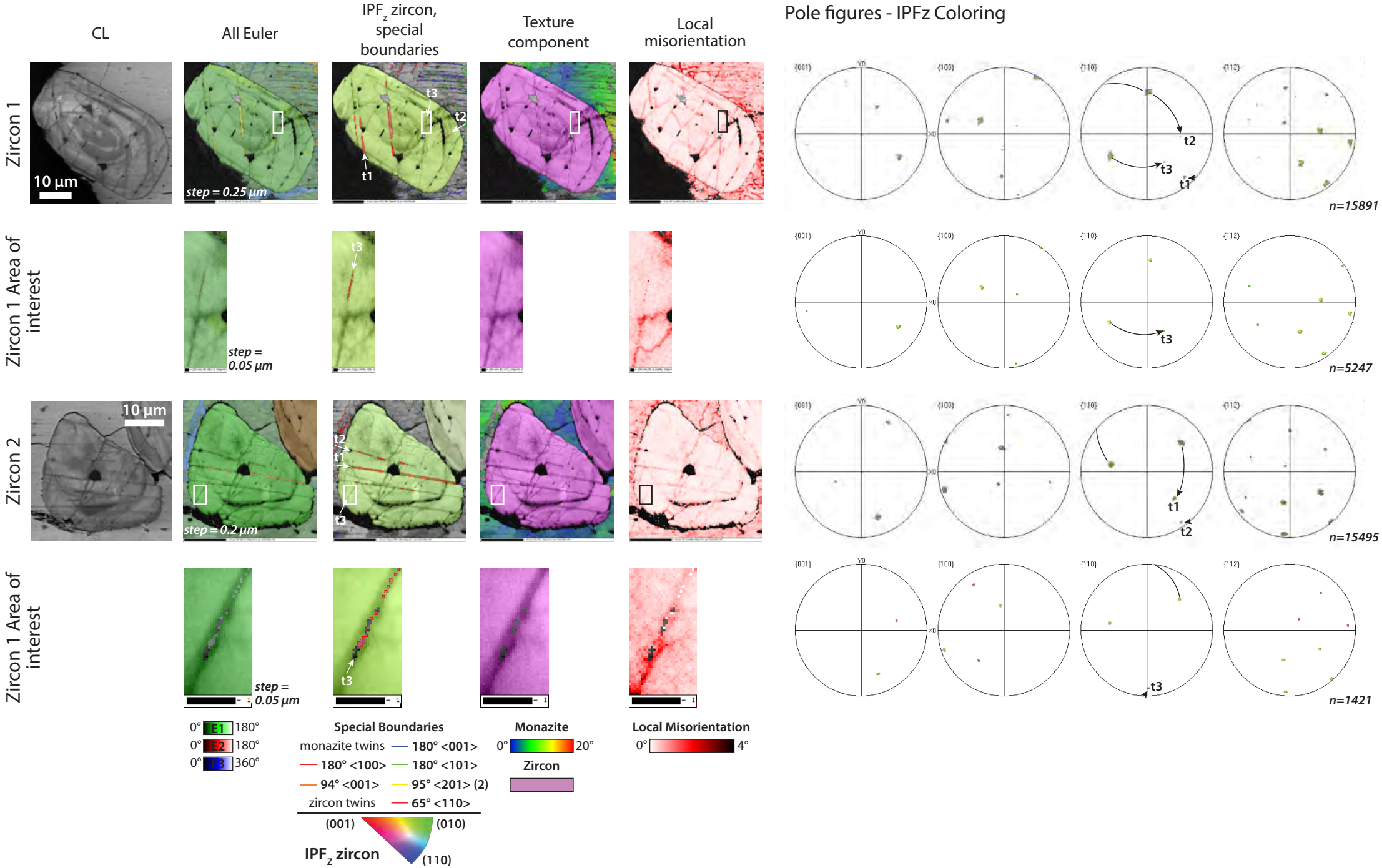

07VD07 - Monazite 39 cont.

Zircon Inclusions

CL | All Euler | IPF_z zircon, special boundaries | Texture component | Local misorientation | Pole figures - IPFz Coloring

Zircon 3

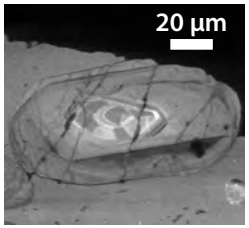

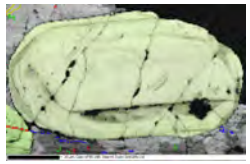

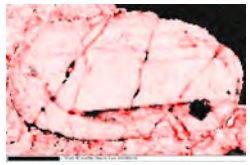

n=14154

Zircon 4

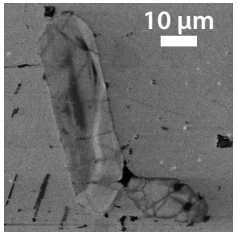

n=3017

Zircon 5

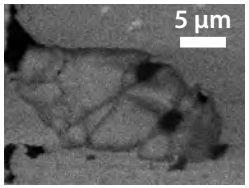

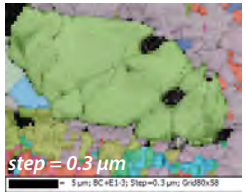

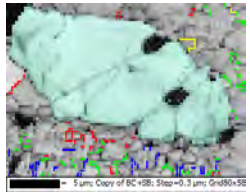

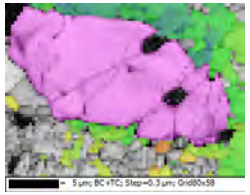

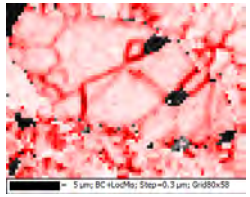

n=2172

Zircon 6

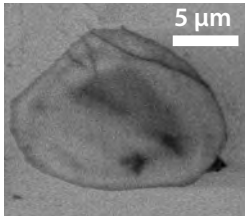

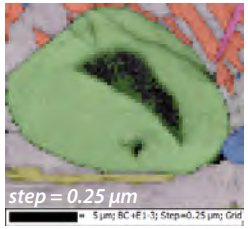

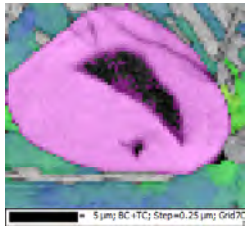

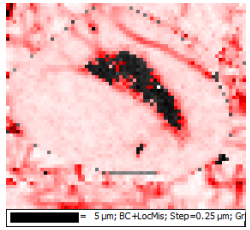

n=2161

Zircon 7, 8

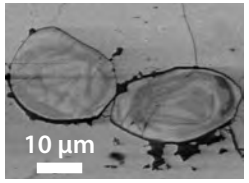

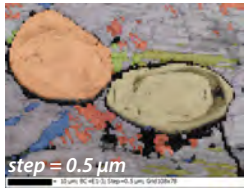

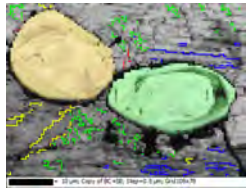

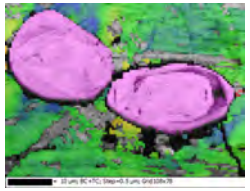

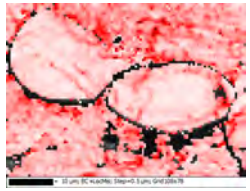

n=1295

n=1409

0° E1 180°
0° E2 180°
0° E3 360°

Special Boundaries

monazite twins
180° <001>
180° <100>
180° <101>
94° <001>
95° <201> (2)
zircon twins
65° <110>

Monazite
0° 20°

Zircon

Local Misorientation
0° 4°

IPF_z zircon

09VD58 - Monazite 166

Rietspruit tributary

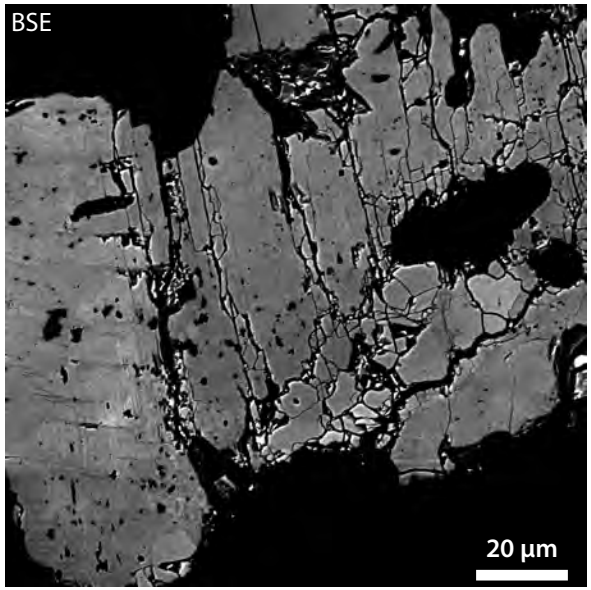

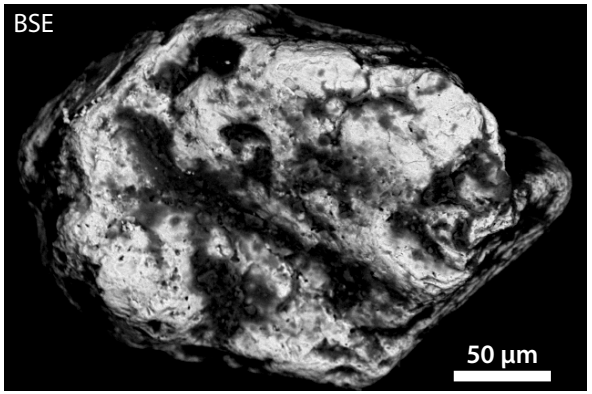

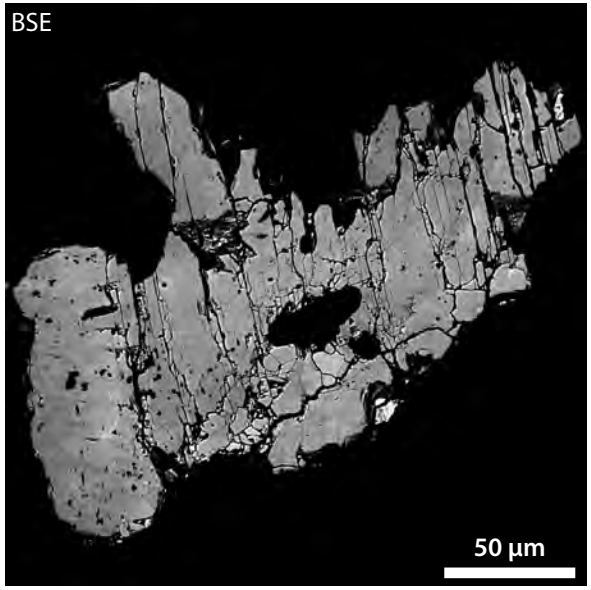

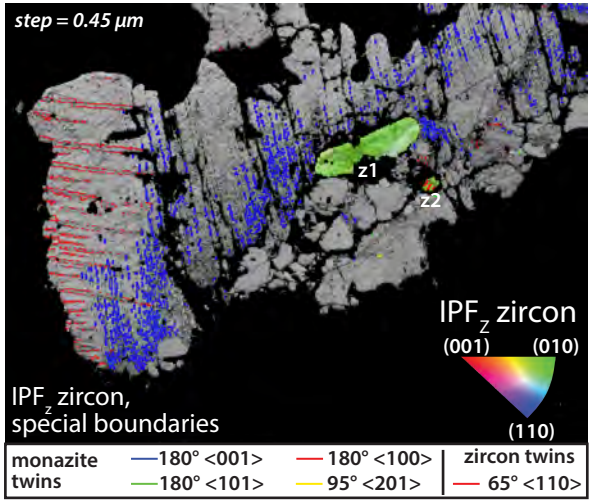

Pole figures - monazite
All Euler coloring

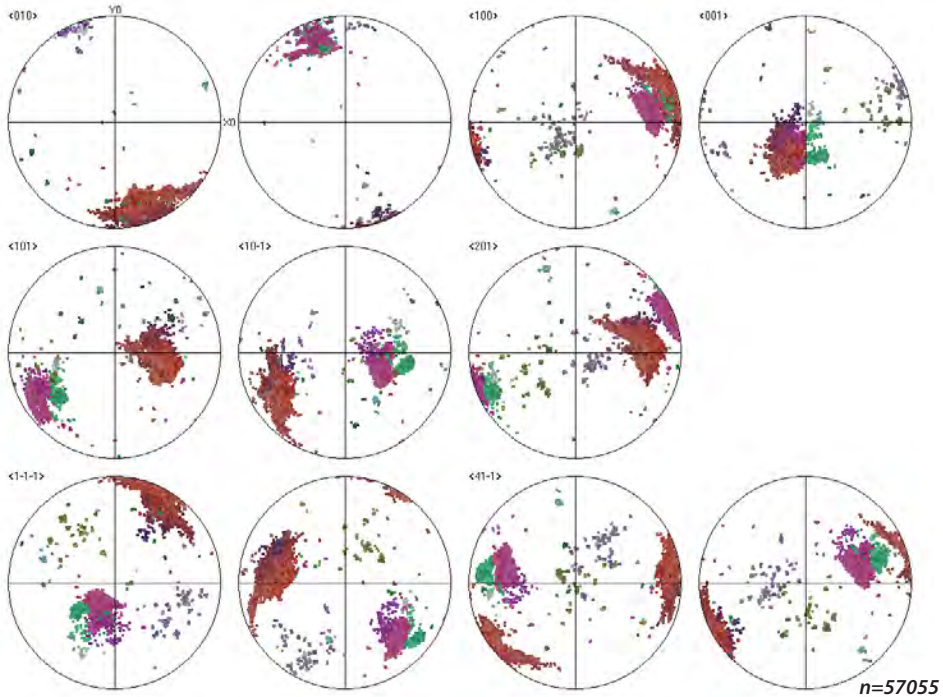

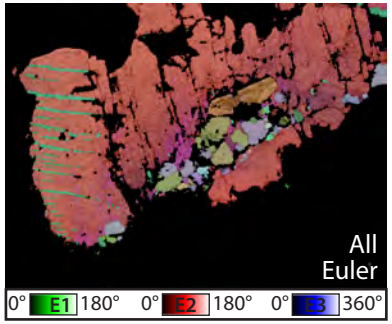

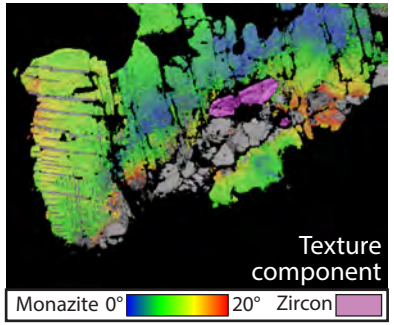

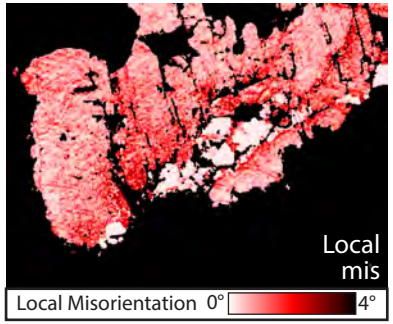

Pole figures - zircon inclusions (n=2)
IPFz Coloring

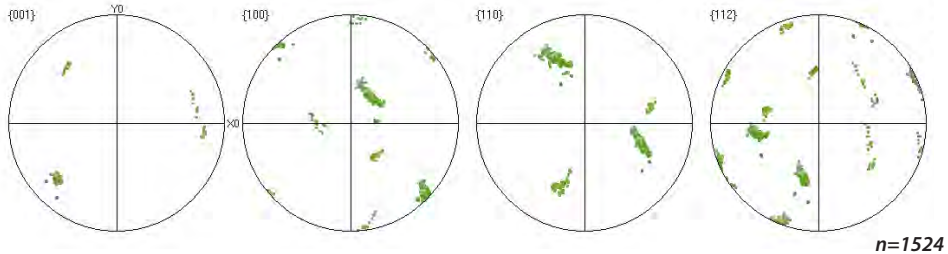

09VD58 - Monazite 166 cont.

Zircon Inclusions

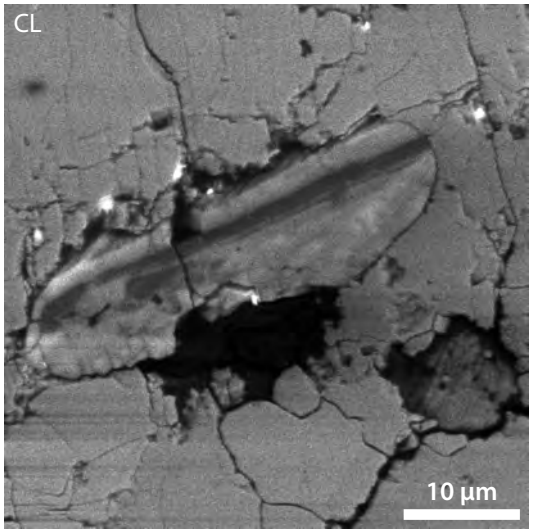

All Euler

IPF$_z$ zircon, special boundaries

Texture component

Local misorientation

Zircons

Zircon 1 Area of interest

Zircon 2

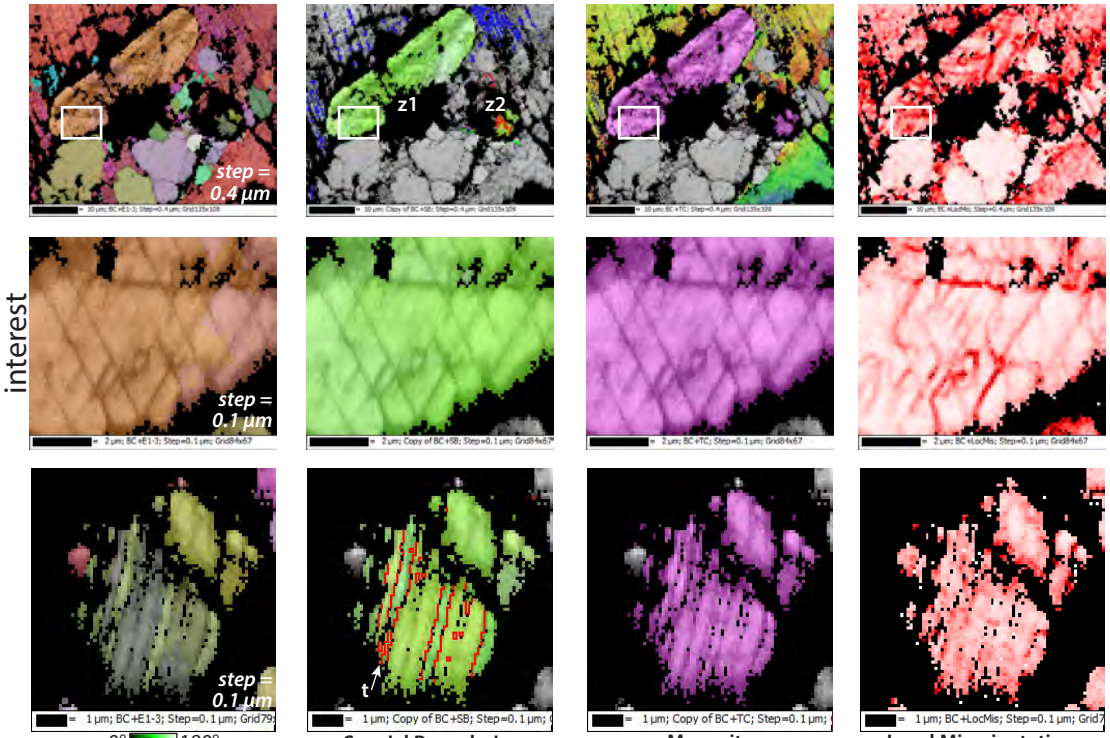

0° E1 180°
0° E2 180°
0° E3 360°

Special Boundaries
monazite twins
180° <001>
180° <100>
180° <101>
95° <201>
zircon twins
65° <110>

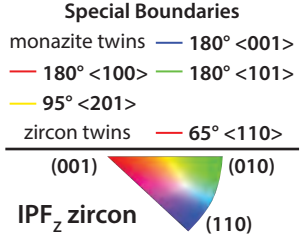

IPF$_z$ zircon

Monazite
0° 20°
Zircon

Local Misorientation
0° 4°

Pole figures - IPFz Coloring

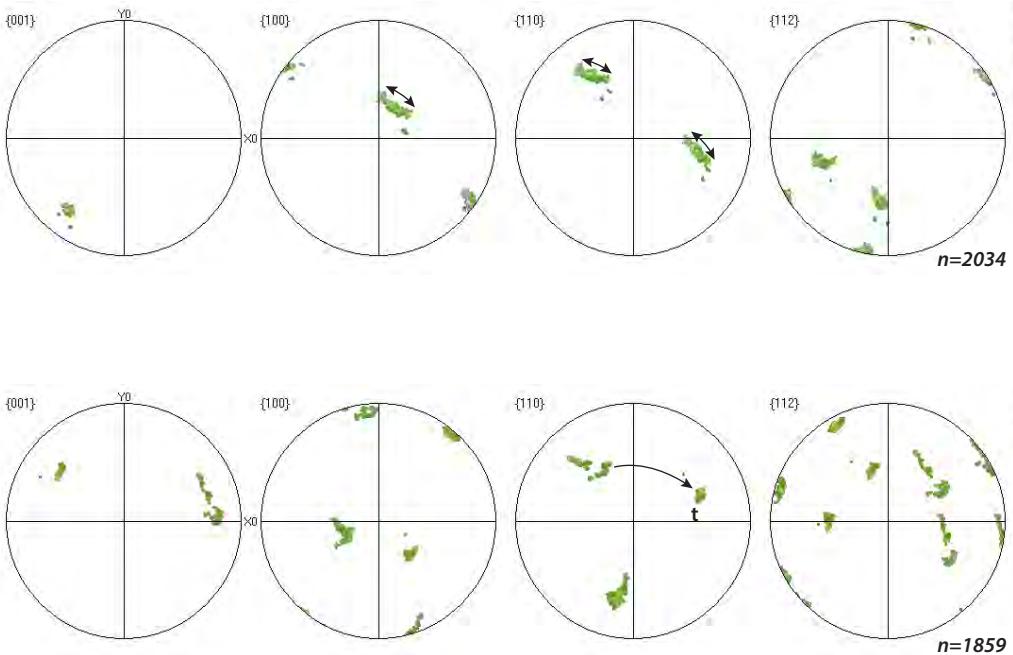

07VD07 - Monazite 67

Rietspruit tributary

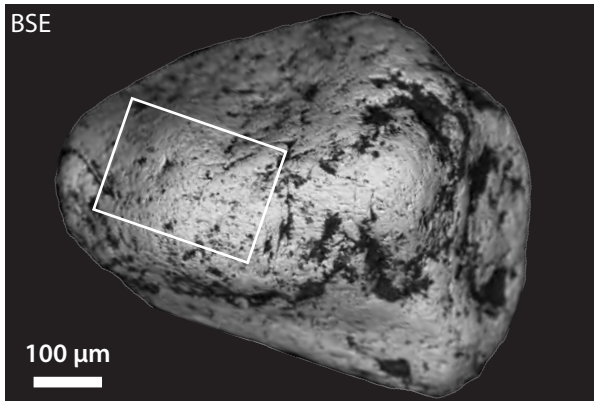

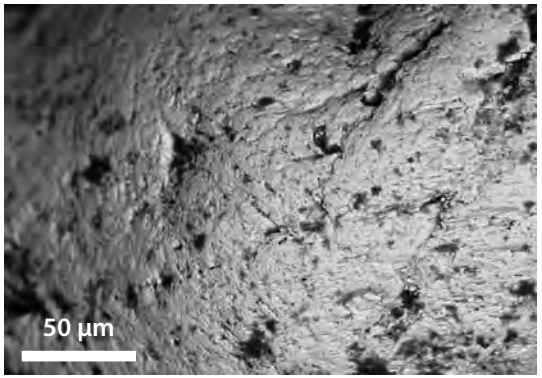

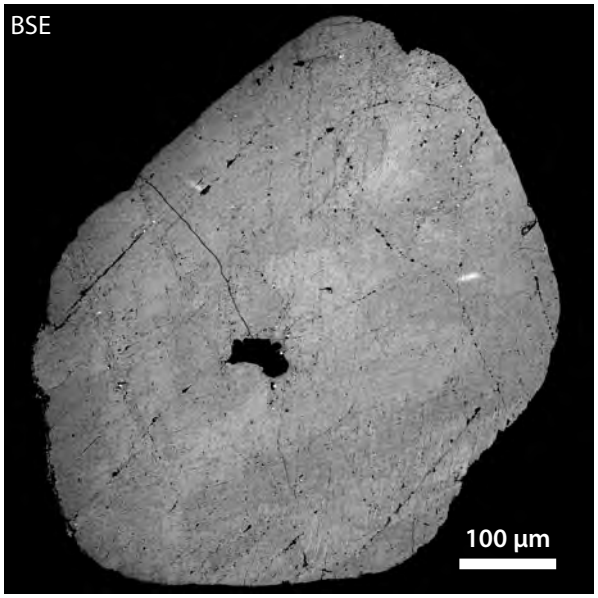

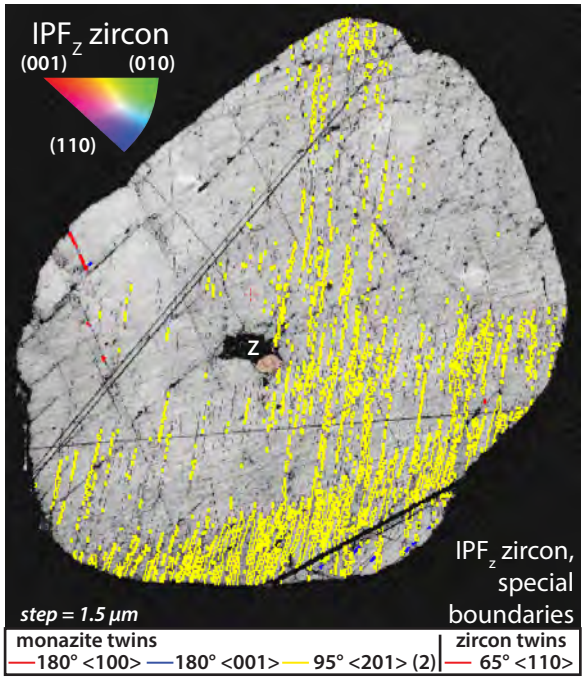

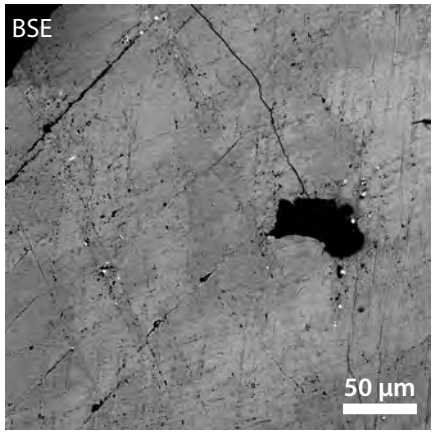

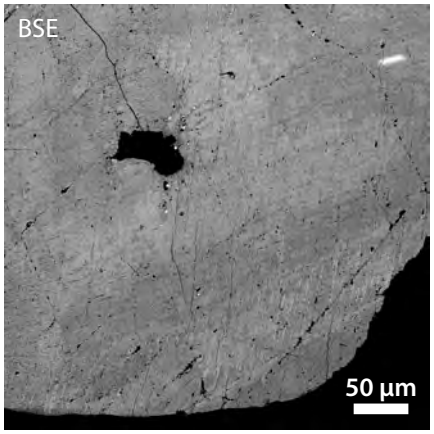

Pole figures - monazite
All Euler coloring

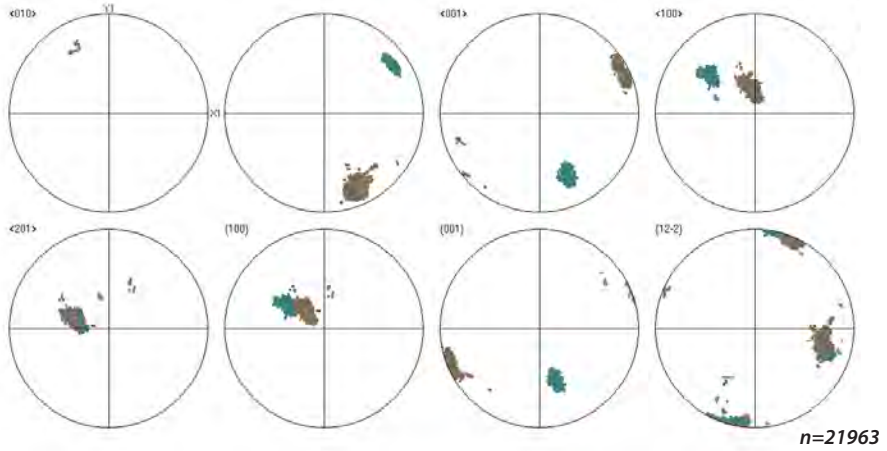

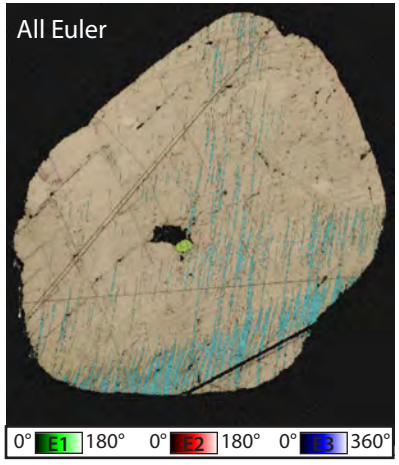

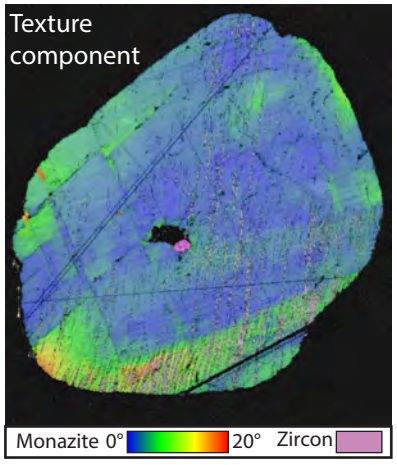

07VD07 - Monazite 67 cont.

Zircon Inclusion

All Euler

IPF_z zircon, special boundaries

Texture component

Local misorientation

Zircon

Zircon Area of interest

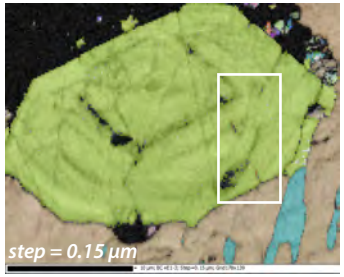

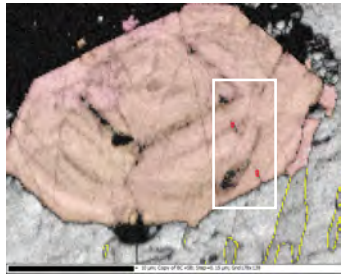

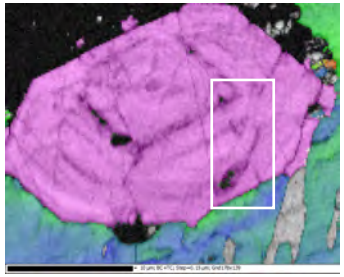

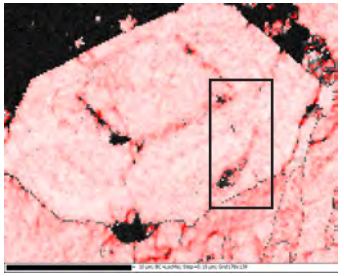

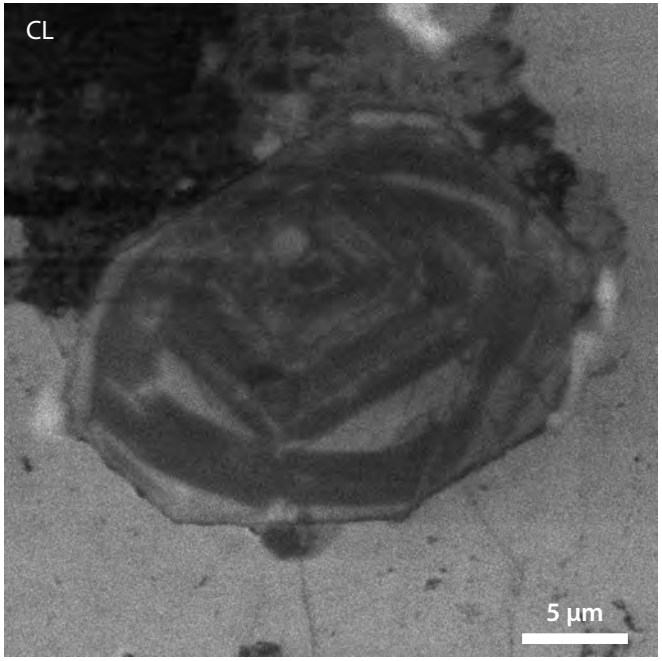

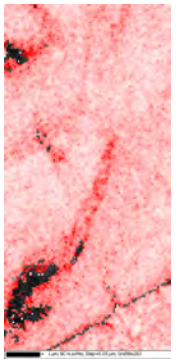

0° E1 180°
0° E2 180°
0° E3 360°

Special Boundaries

monazite twins — 180° <001>
— 180° <100> — 95° <201> (2)
zircon twins — 65° <110>

IPF_z zircon

Monazite

0° 20°

Zircon

Local Misorientation

0° 4°

Pole figures - IPFz Coloring

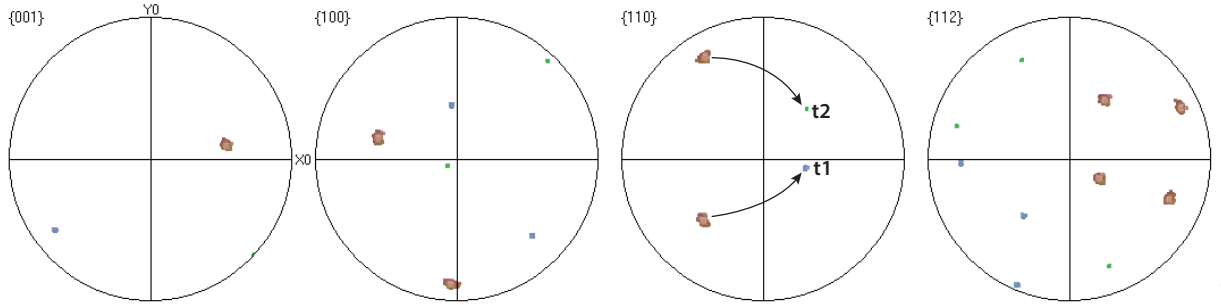

n=17673

07VD08 - Monazite 4 Vaal River - 39 km downriver

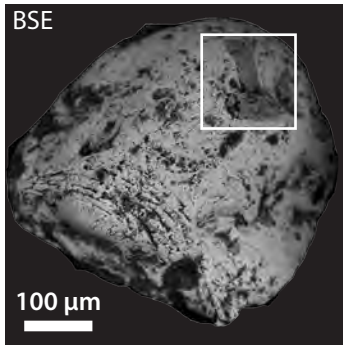

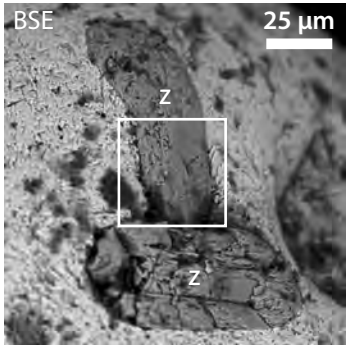

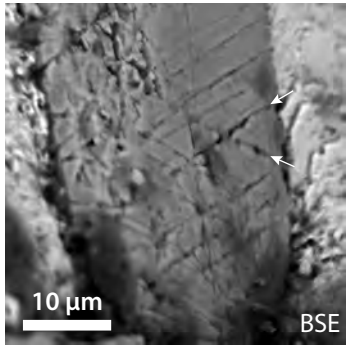

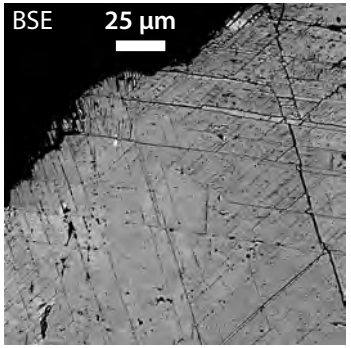

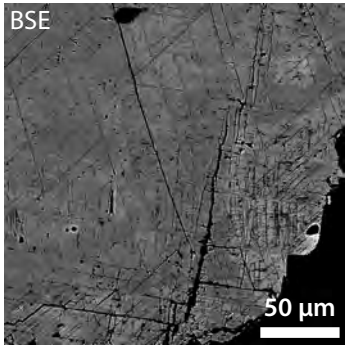

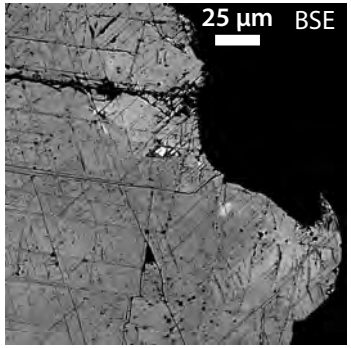

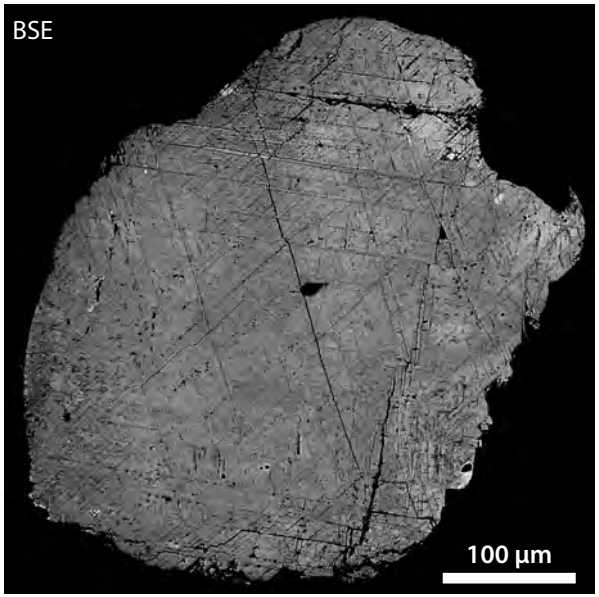

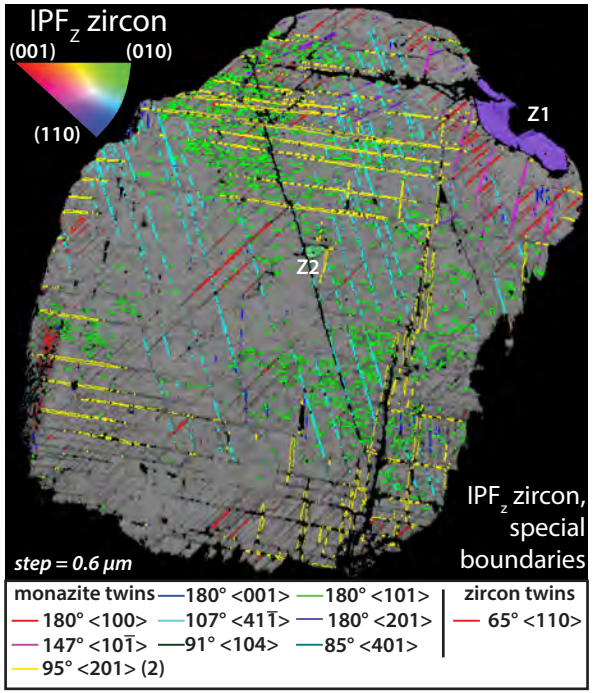

Pole figures - monazite
All Euler coloring

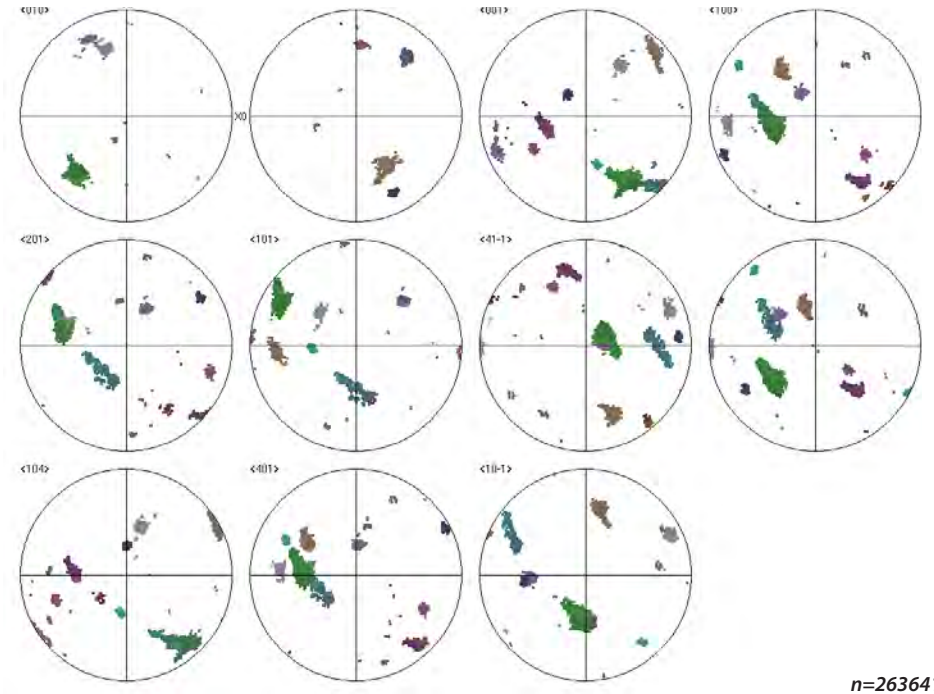

n=263641

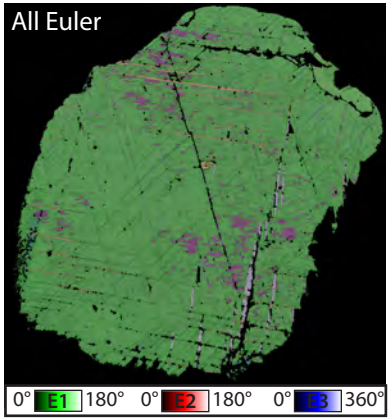

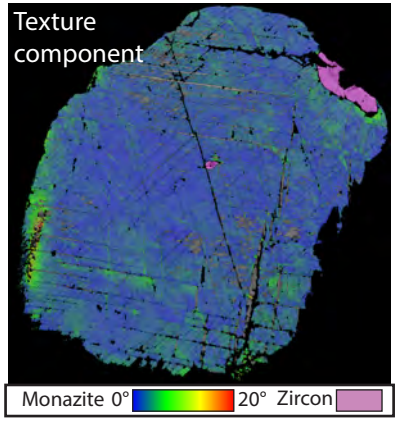

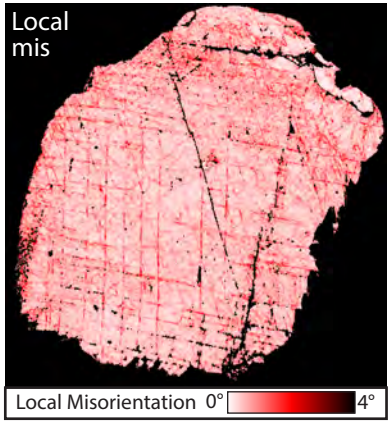

Pole figures - zircon inclusions (n=2)
IPFz Coloring

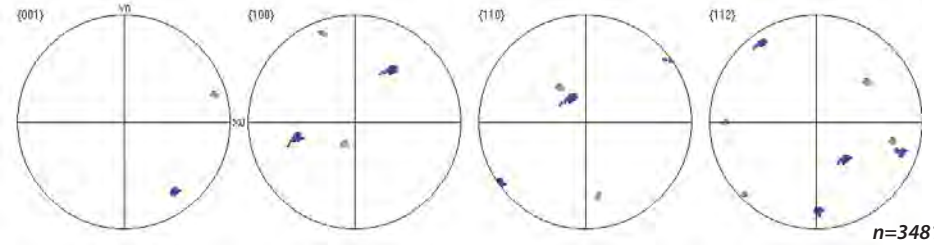

n=3481

07VD08 - Monazite 4 cont.

Zircon Inclusions

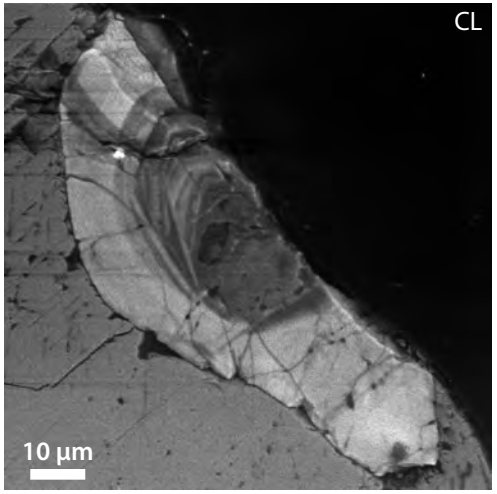

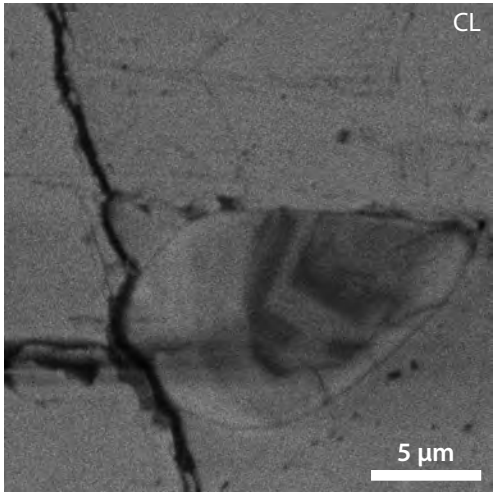

All Euler | IPF$_z$ zircon, special boundaries | Texture component | Local misorientation

Zircon 1

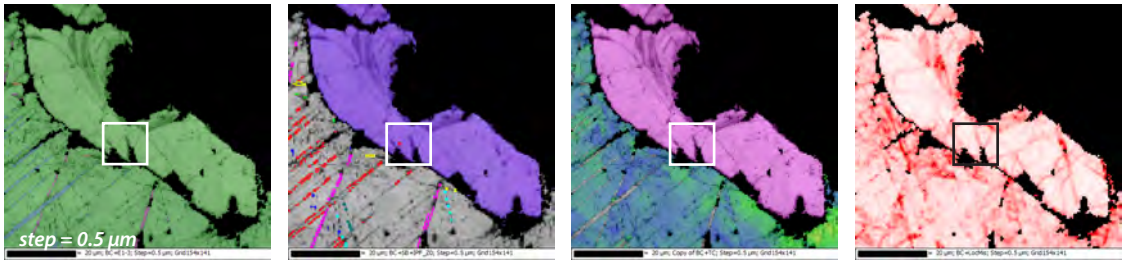

Zircon 1 Area of interest

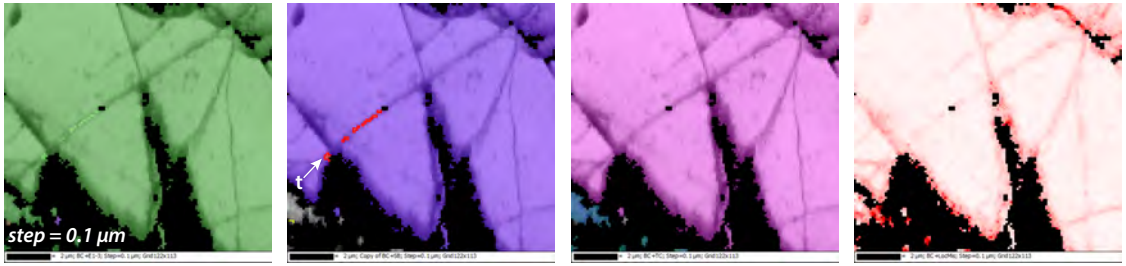

Zircon 2

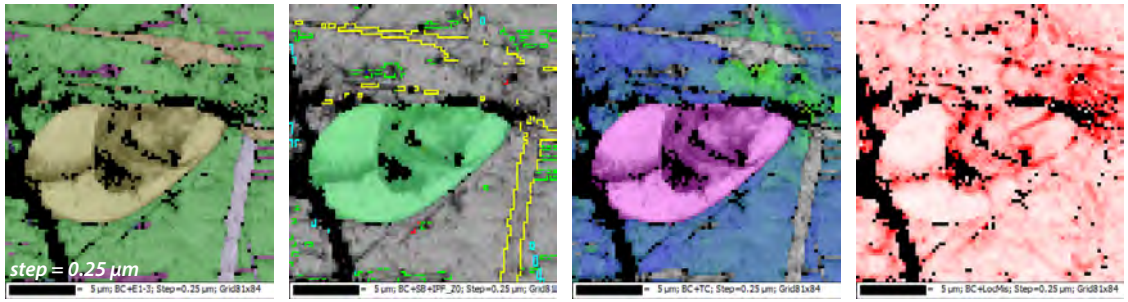

Pole figures - IPFz Coloring

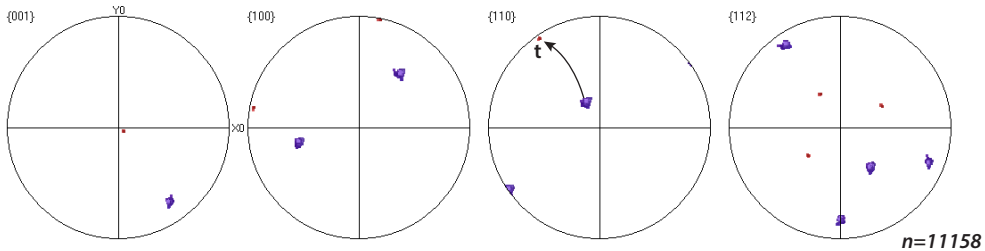

n=11158

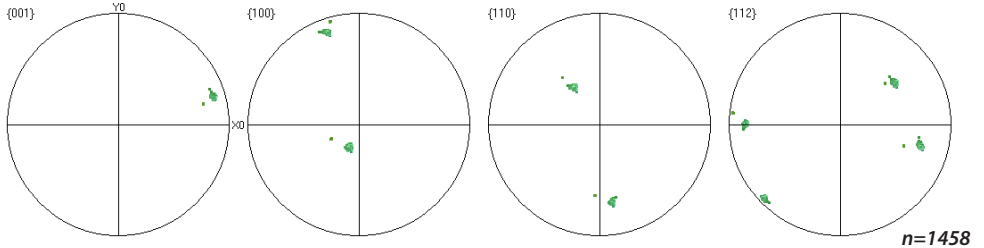

n=1458

0° E1 180°
0° E2 180°
0° E3 360°

Special Boundaries
monazite twins
180° <100> | 180° <001>
107° <41$\bar{1}$> | 180° <101>
147° <10$\bar{1}$> | 95° <201> (2)
85° <401> | 180° <201>
zircon twins | 65° <110>

Monazite
0° 20°
Zircon

Local Misorientation
0° 4°

IPF$_z$ zircon

09VD16 - Monazite 50

Vaal River - 103 km downriver

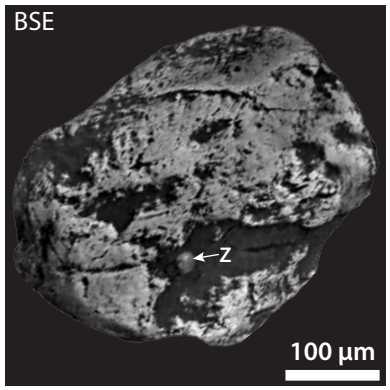

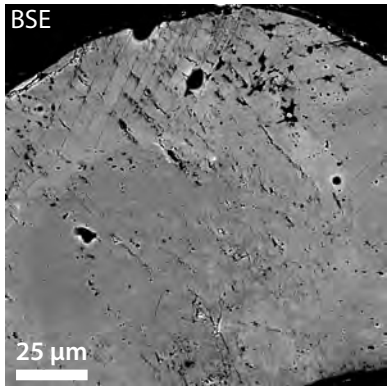

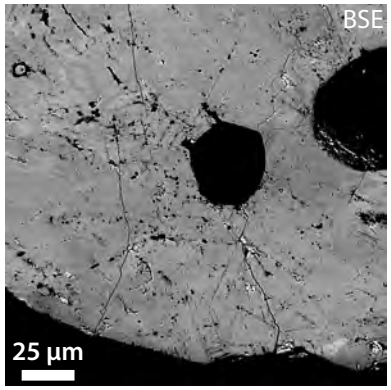

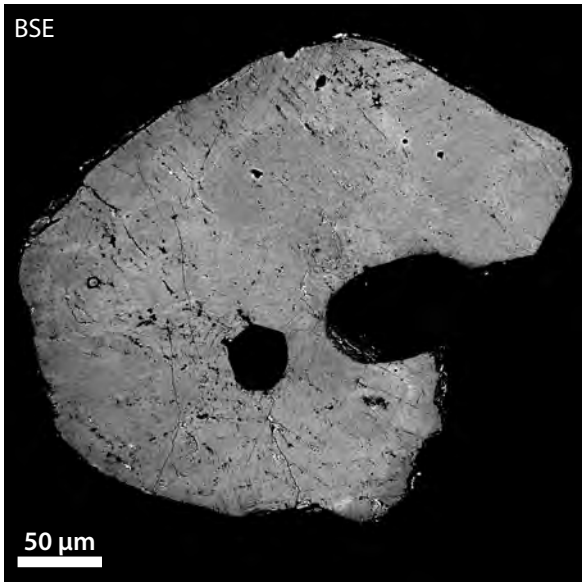

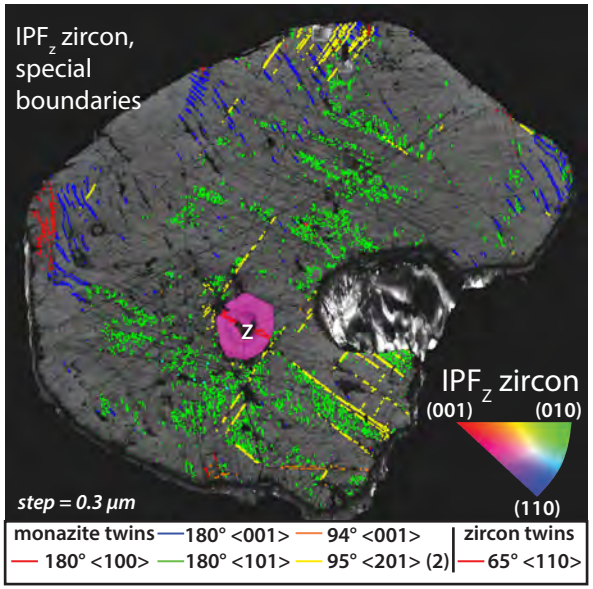

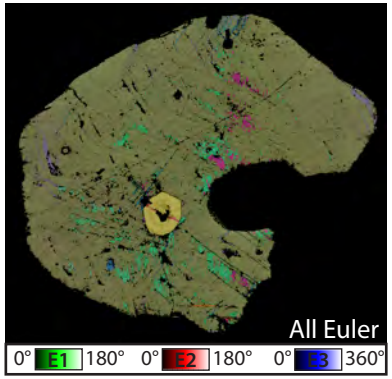

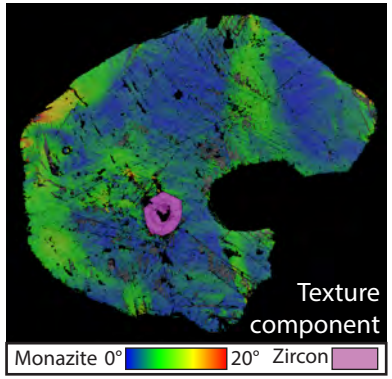

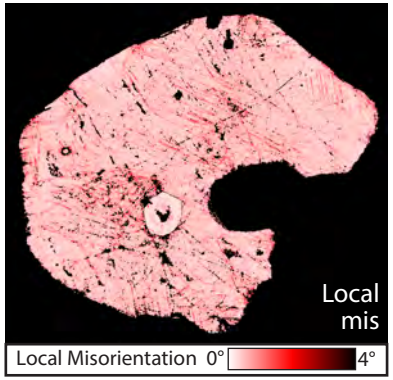

Pole figures - monazite
All Euler coloring

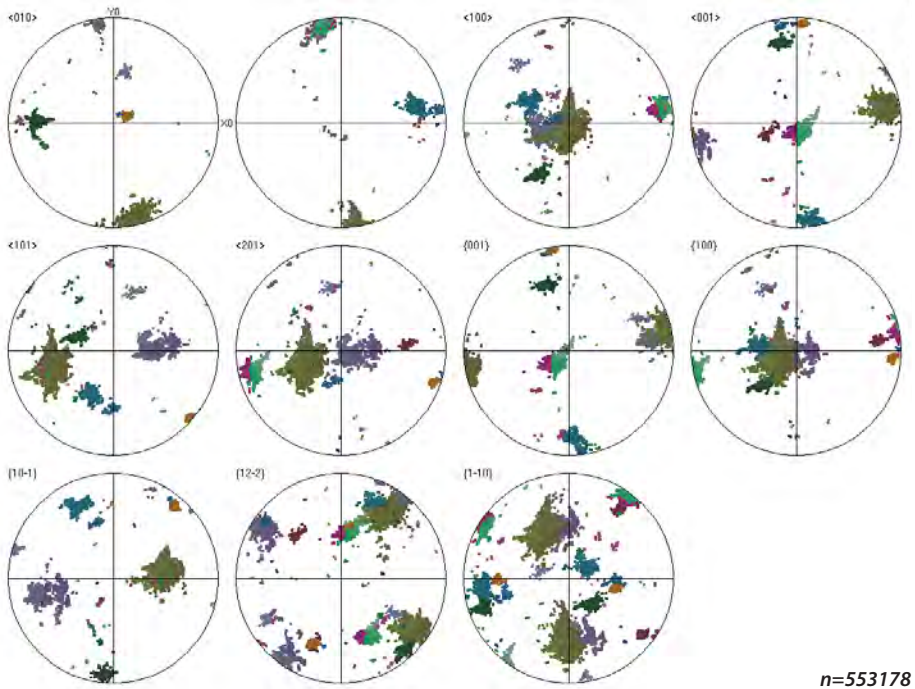

n=553178

09VD16- Monazite 50 cont.

Zircon Inclusion

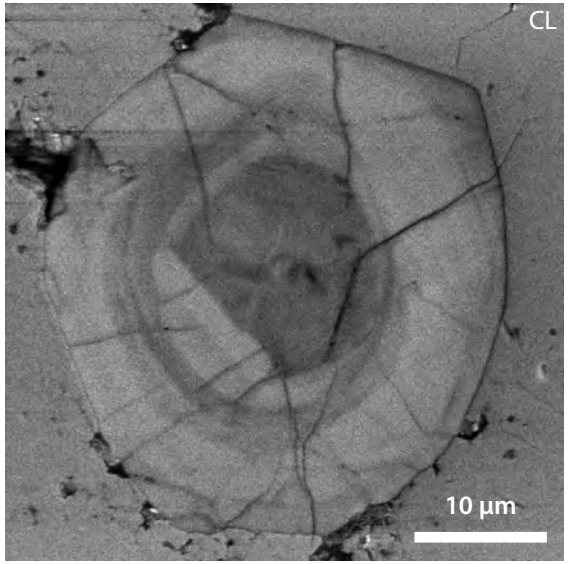

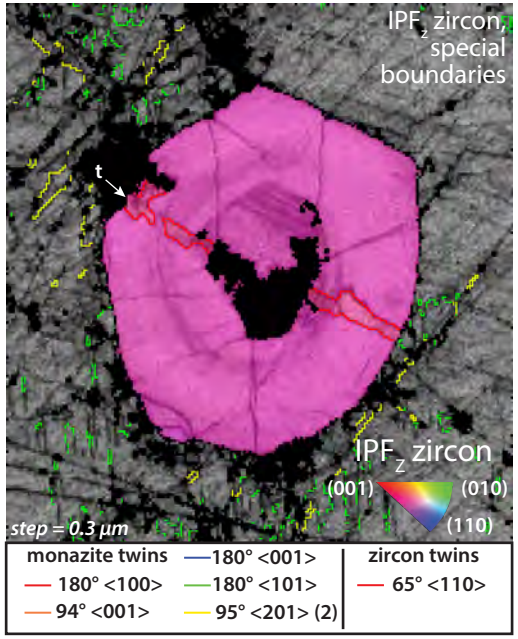

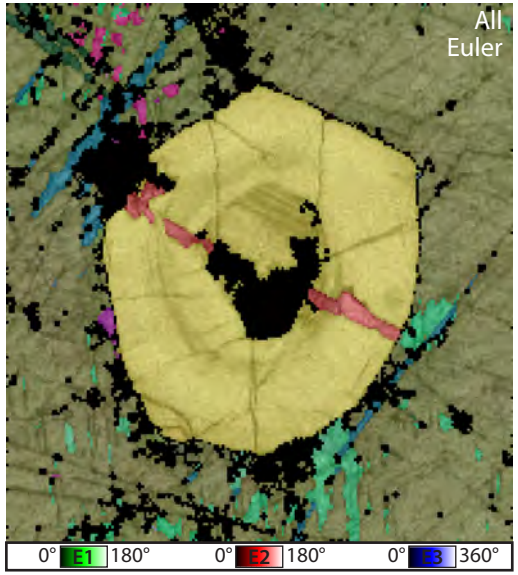

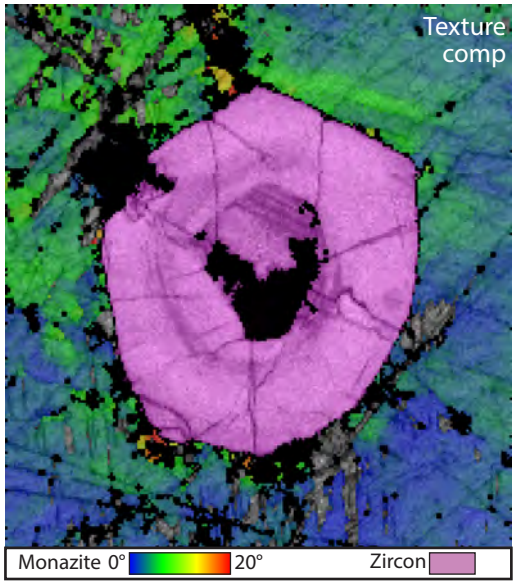

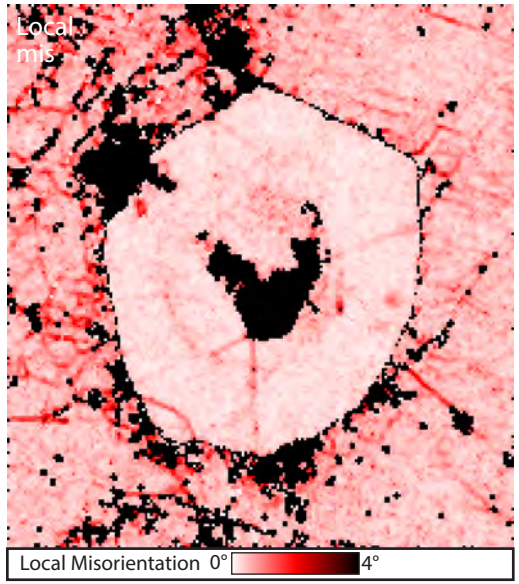

Pole figures - IPFz Coloring

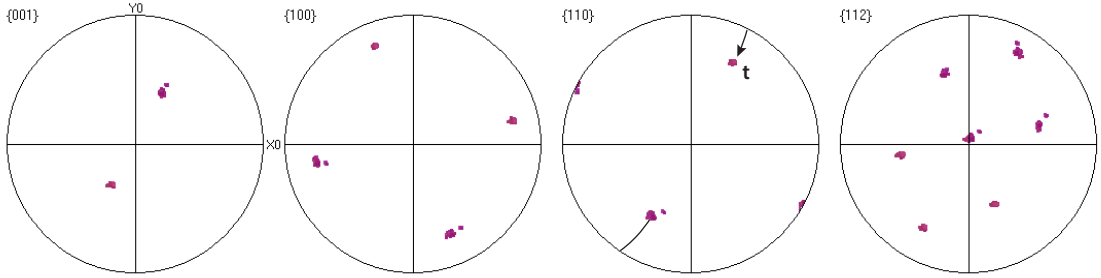

n=10820

09VD16 - Monazite 65

Vaal River - 103 km downriver

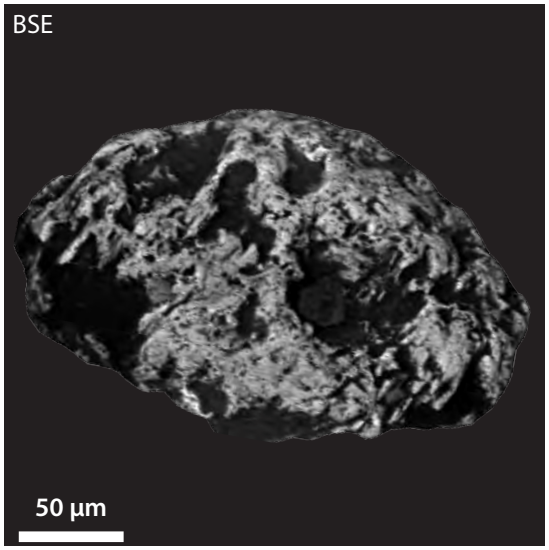

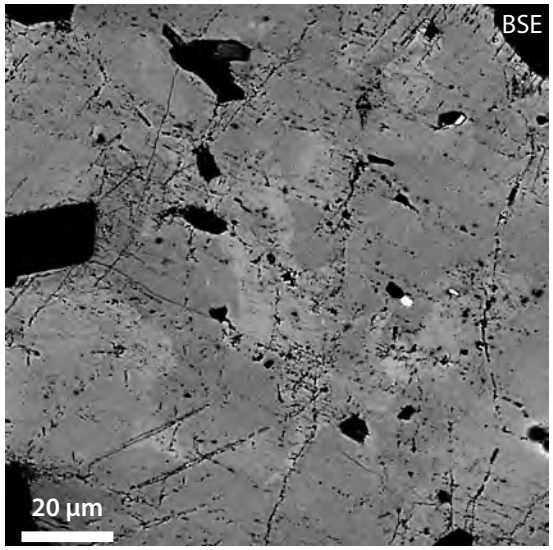

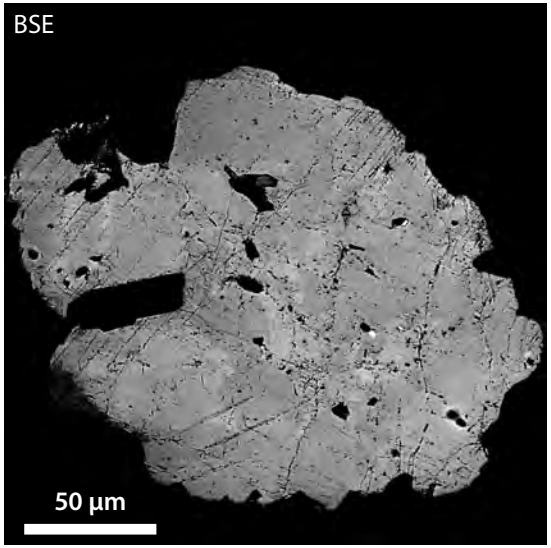

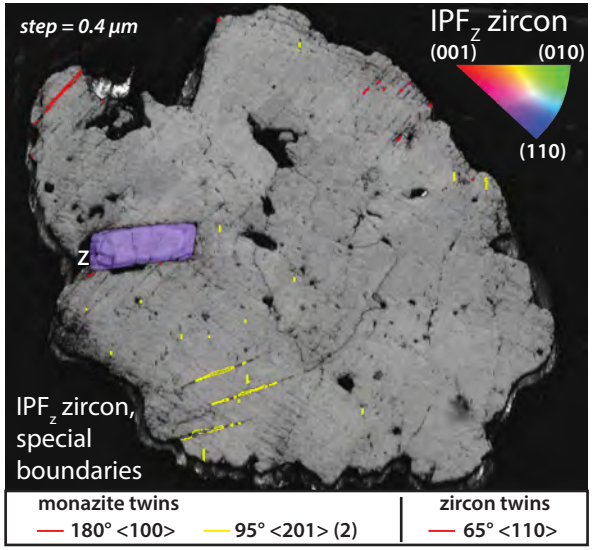

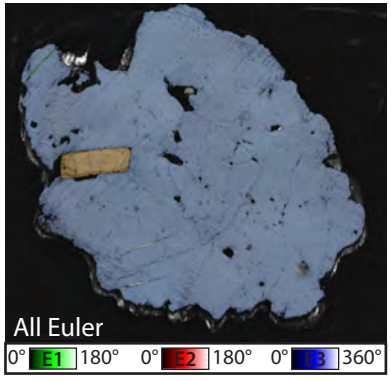

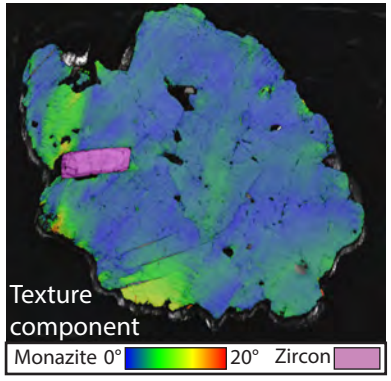

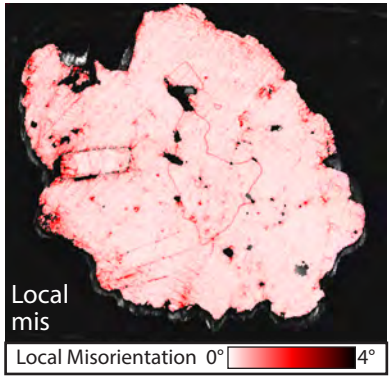

Pole figures - monazite
All Euler coloring

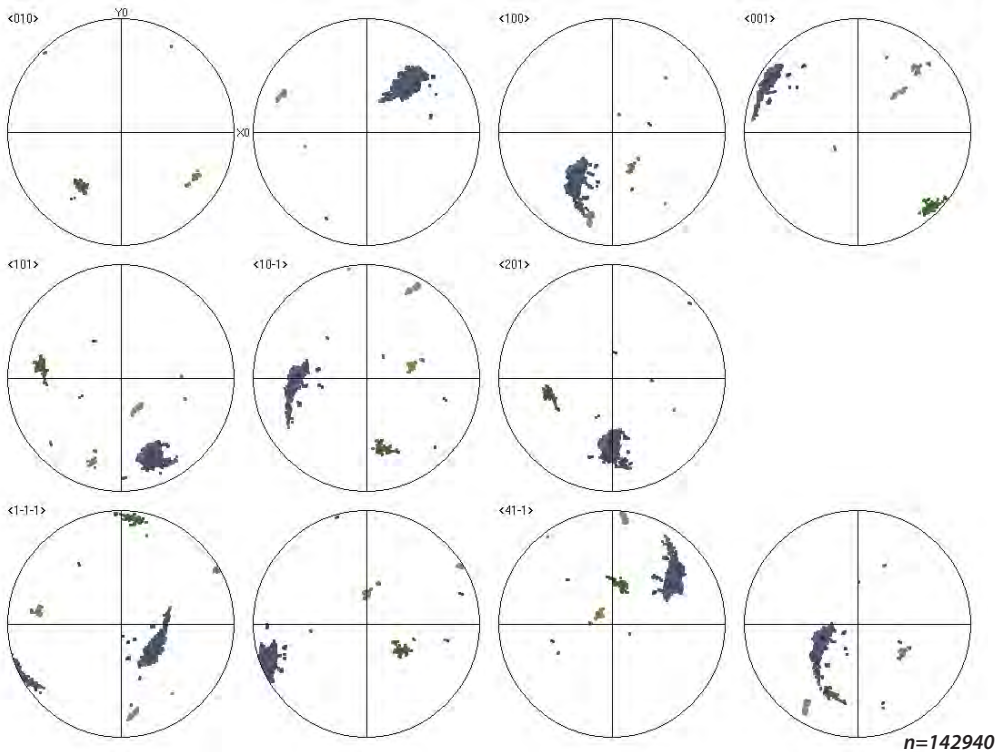

09VD16 - Monazite 65 cont.

Zircon Inclusion

All Euler

IPF$_z$ zircon, special boundaries

Texture component

Local misorientation

Zircon

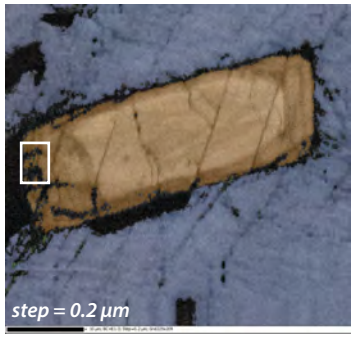

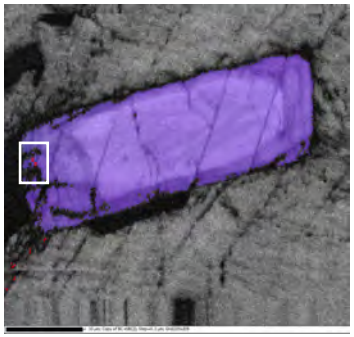

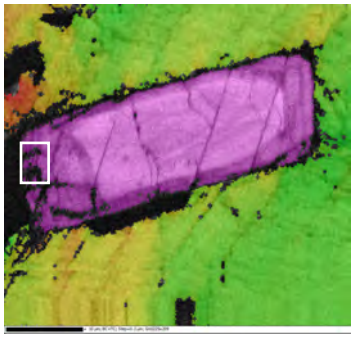

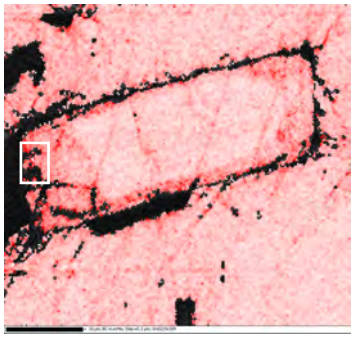

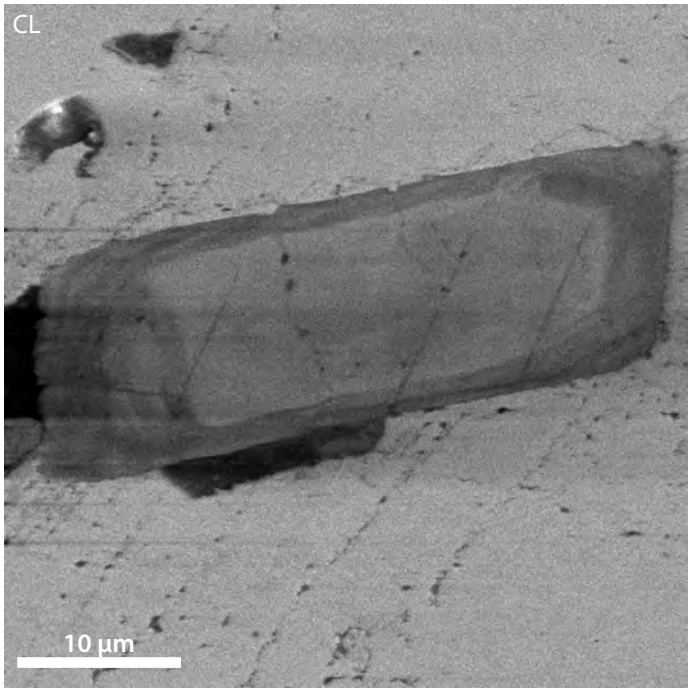

Zircon Area of interest

step = 0.1 µm

0° E1 180°
0° E2 180°
0° E3 360°

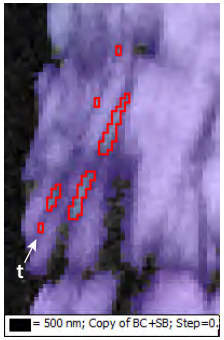

Special Boundaries

monazite twins

180° <100> 95° <201> (2)

zircon twins 65° <110>

IPF$_z$ zircon

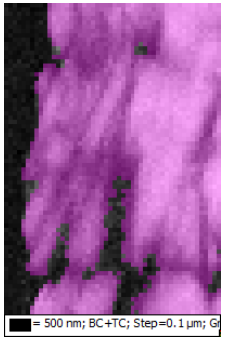

Monazite

0° 20°

Zircon

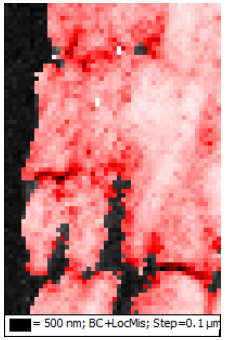

Local Misorientation

0° 4°

Pole figures - IPFz Coloring

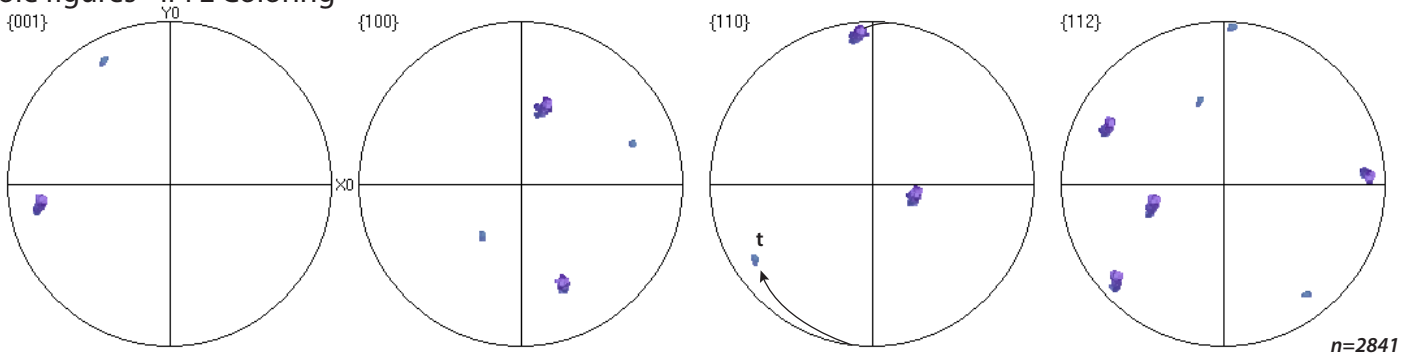

09VD16 - Monazite 68

Vaal River - 103 km downriver

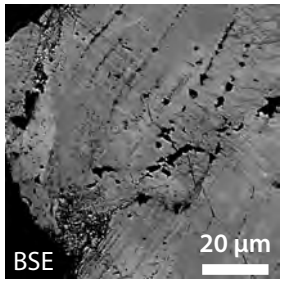

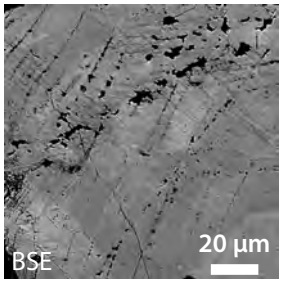

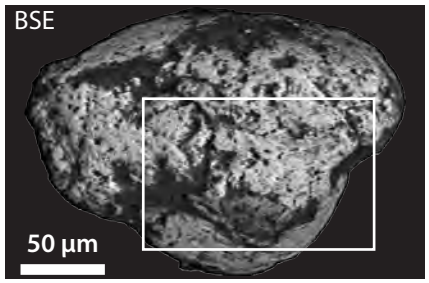

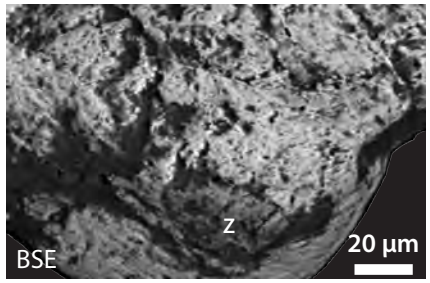

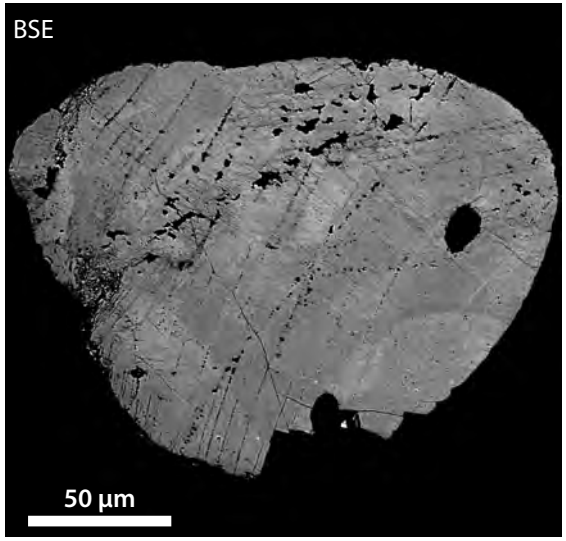

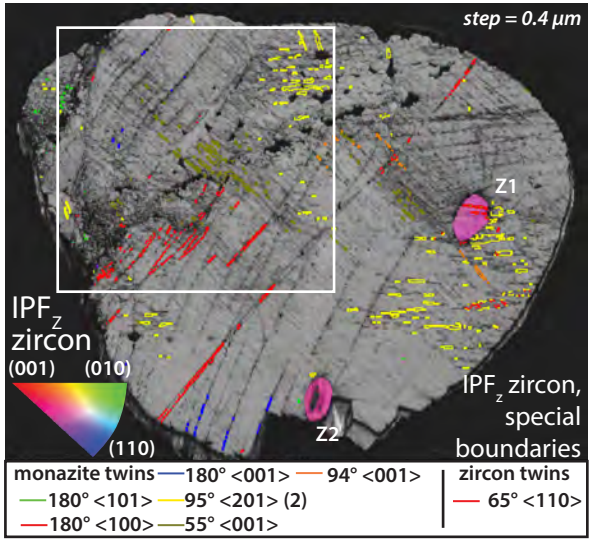

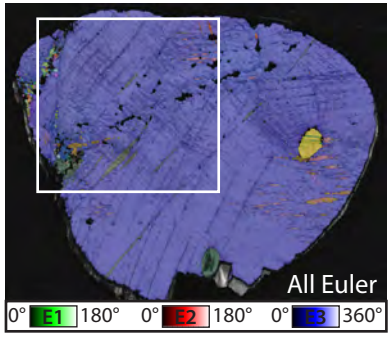

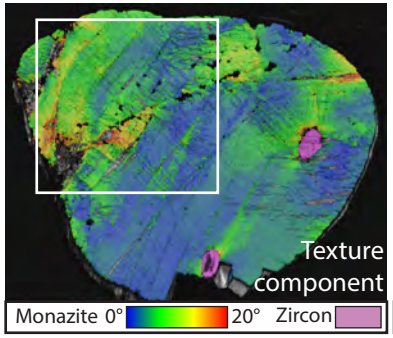

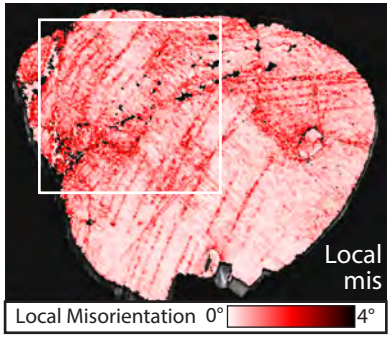

Pole figures - monazite
All Euler coloring

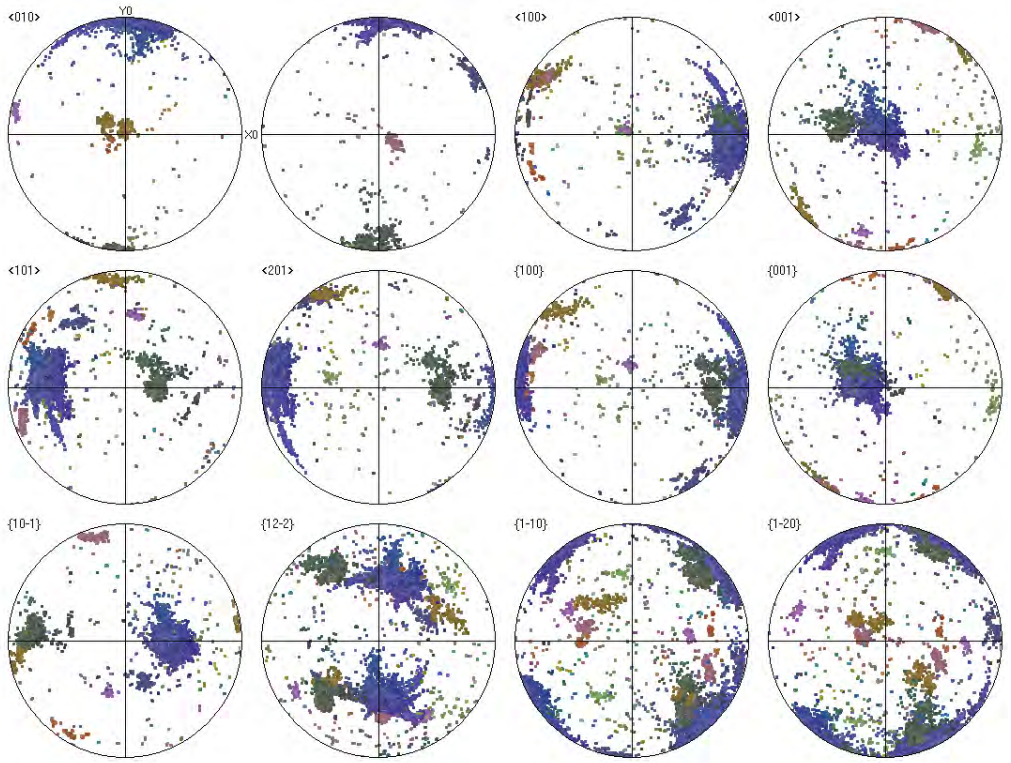

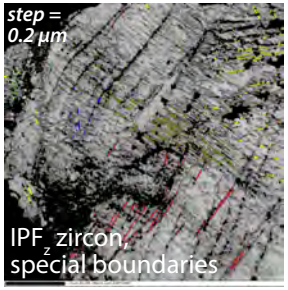

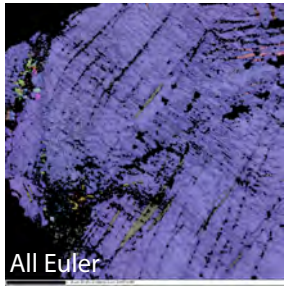

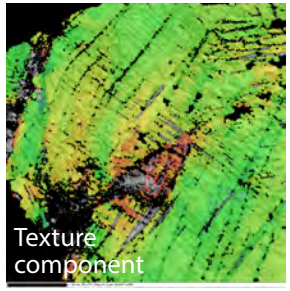

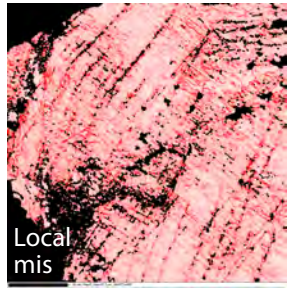

Pole figures - zircon inclusions (n=2)
IPFz Coloring

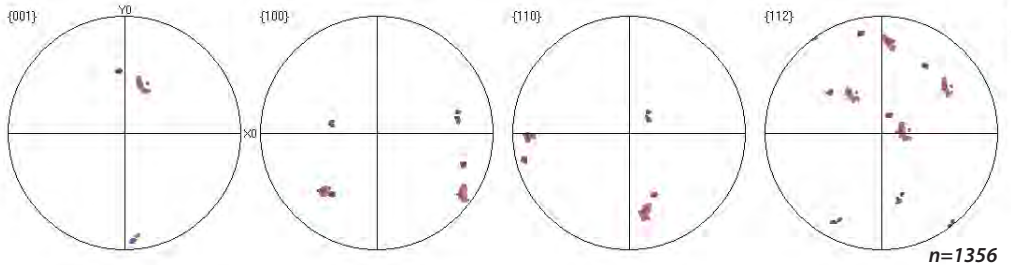

09VD16 - Monazite 68 cont.

Zircon Inclusions

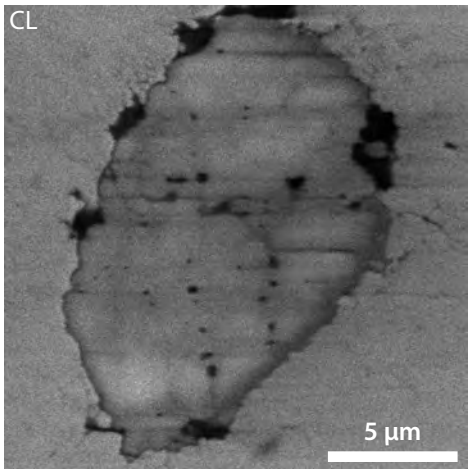

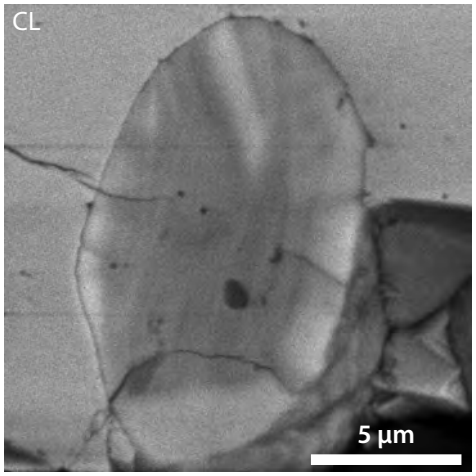

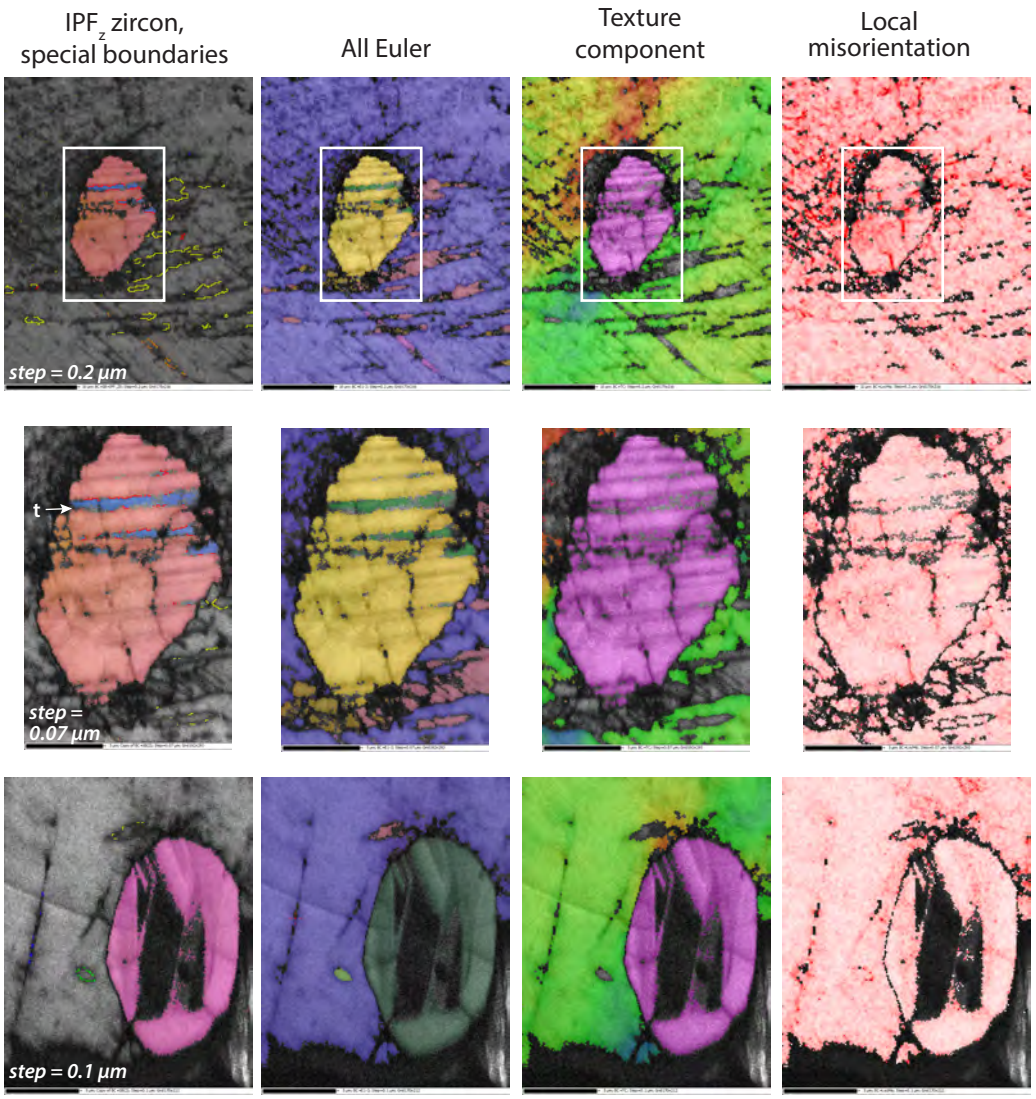

Zircon pole figures - IPFz Coloring

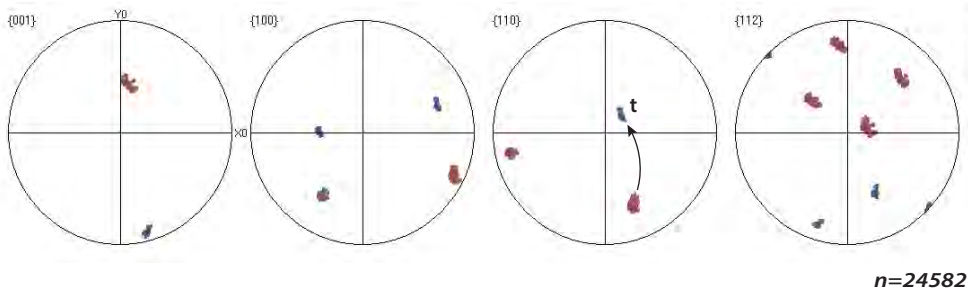

n=24582

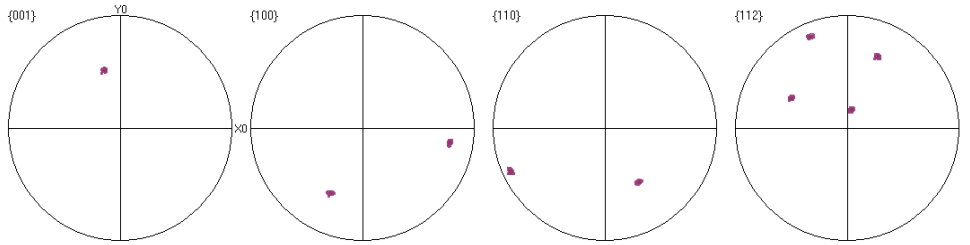

n=6568

09VD53 - Monazite 26

Vaal River - 469 km downriver

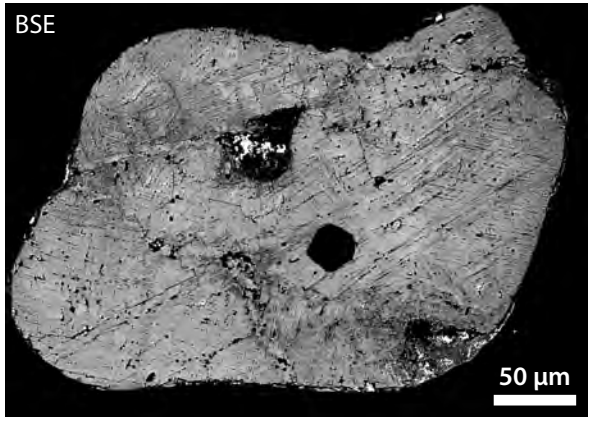

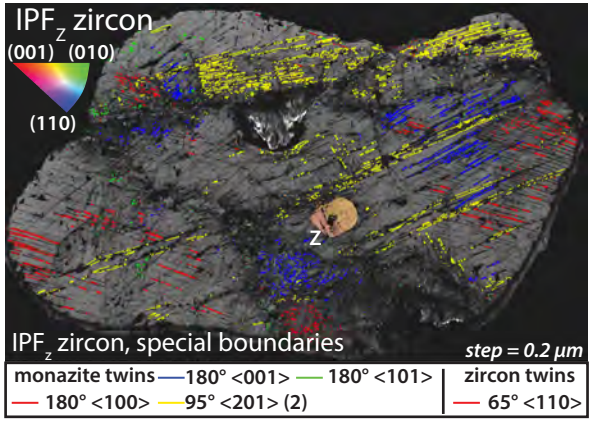

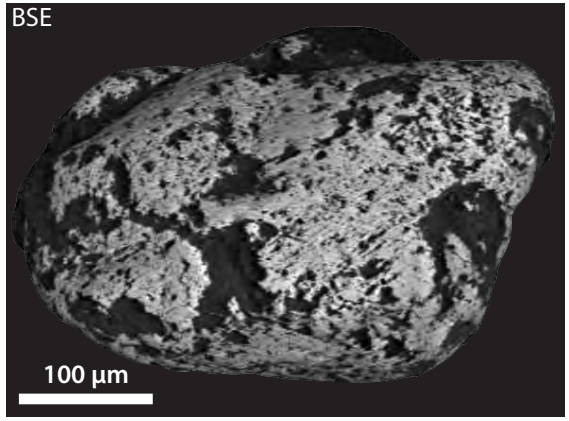

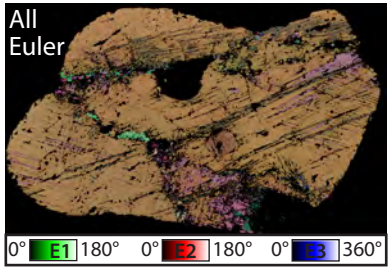

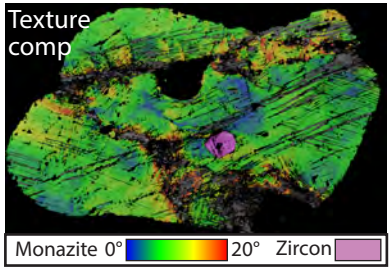

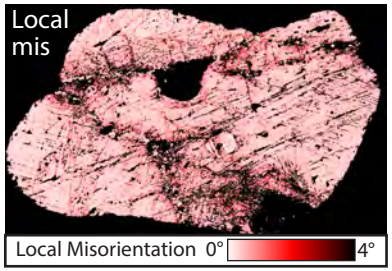

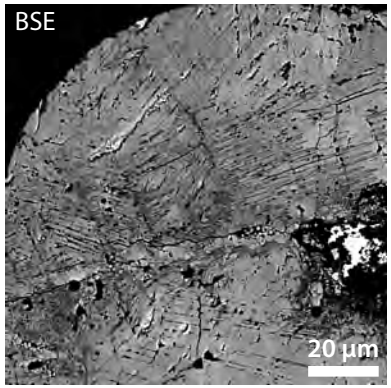

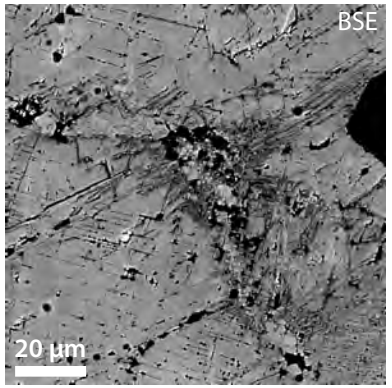

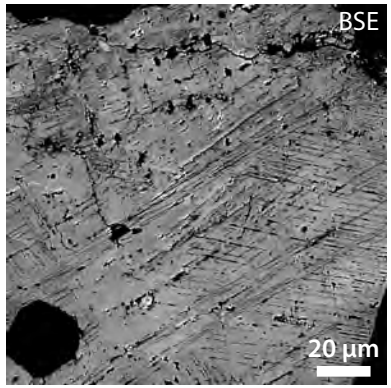

Pole figures - monazite
All Euler coloring

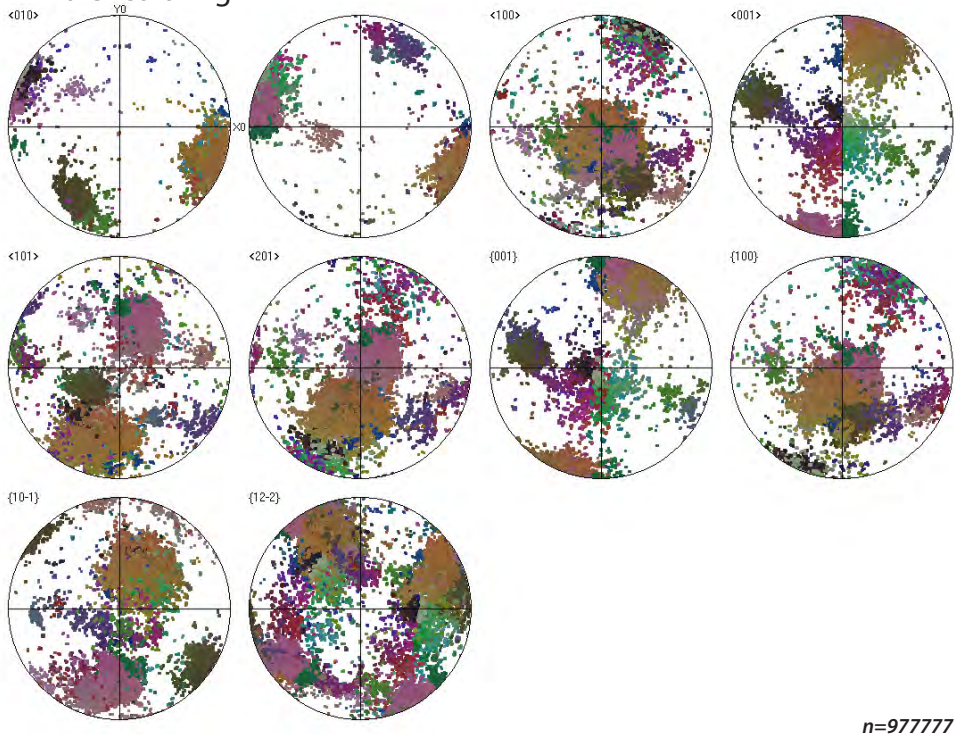

n=977777

09VD53 - Monazite 26 cont.

Zircon Inclusion

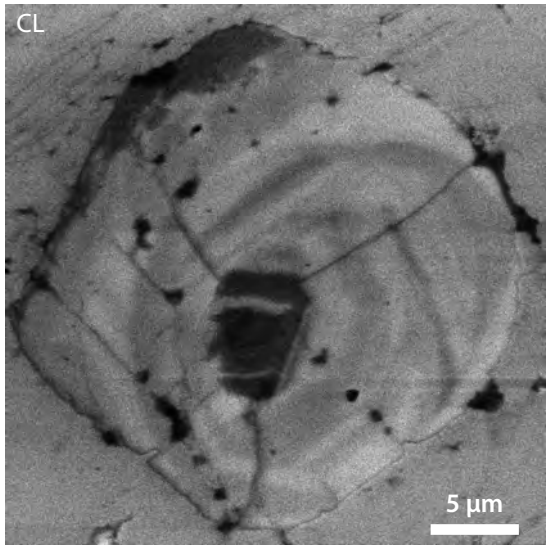

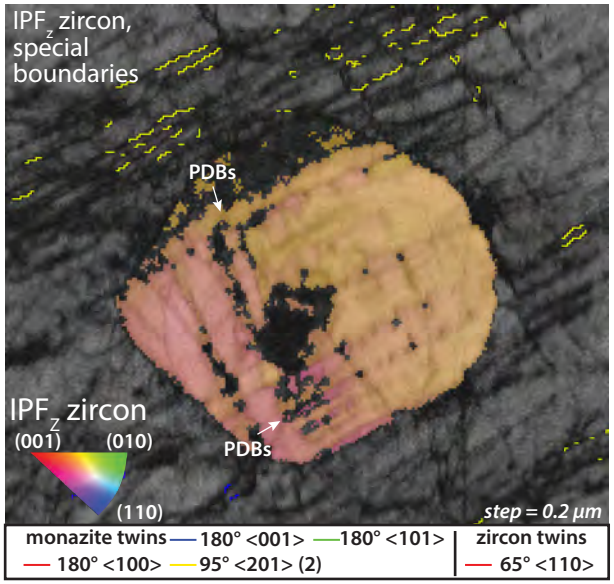

Pole figures - IPFz Coloring

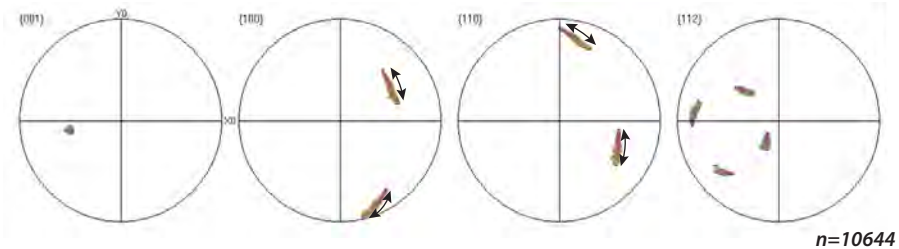

n=10644

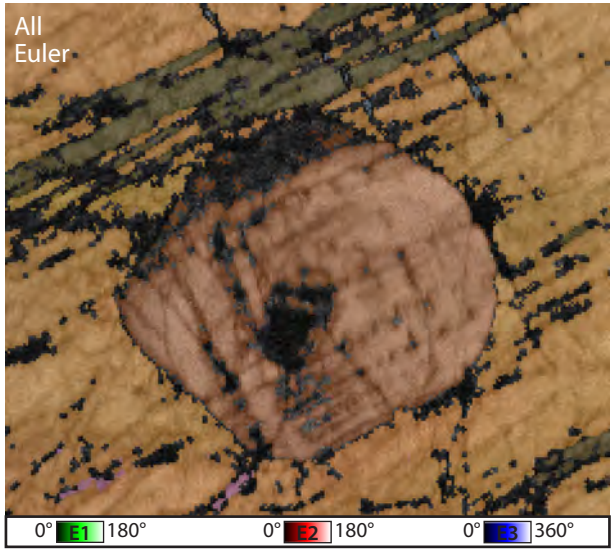

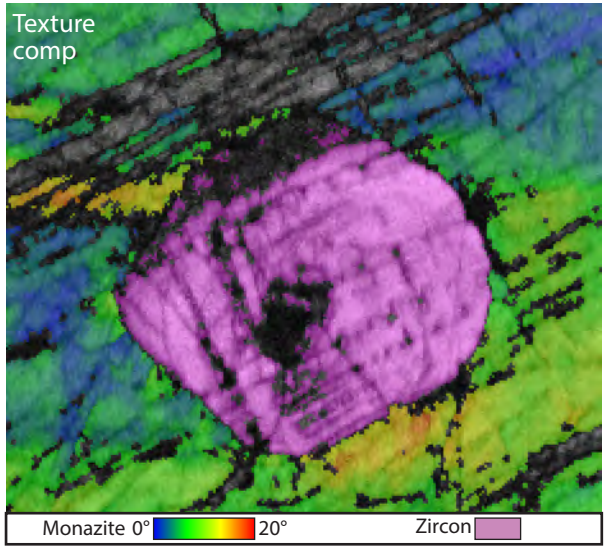

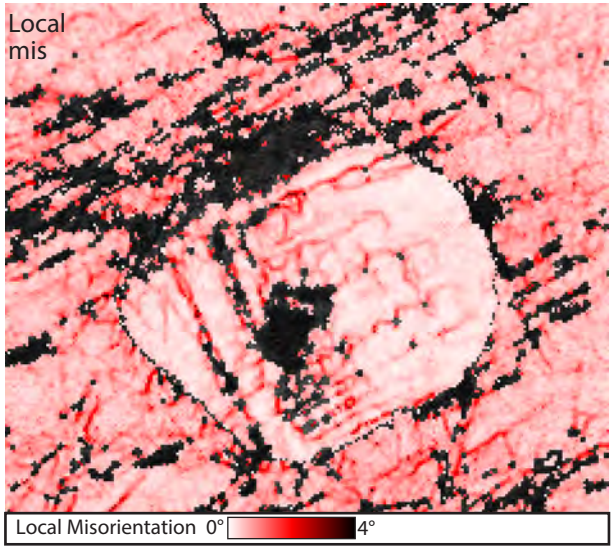

Data Repository 3

2016205_DR3_Twinpairs.xlsx